iScience

CellPress
OPEN ACCESS

Article

A modular hydrogel bioink containing microsphere-embedded chondrocytes for 3D-printed multiscale composite scaffolds for cartilage repair

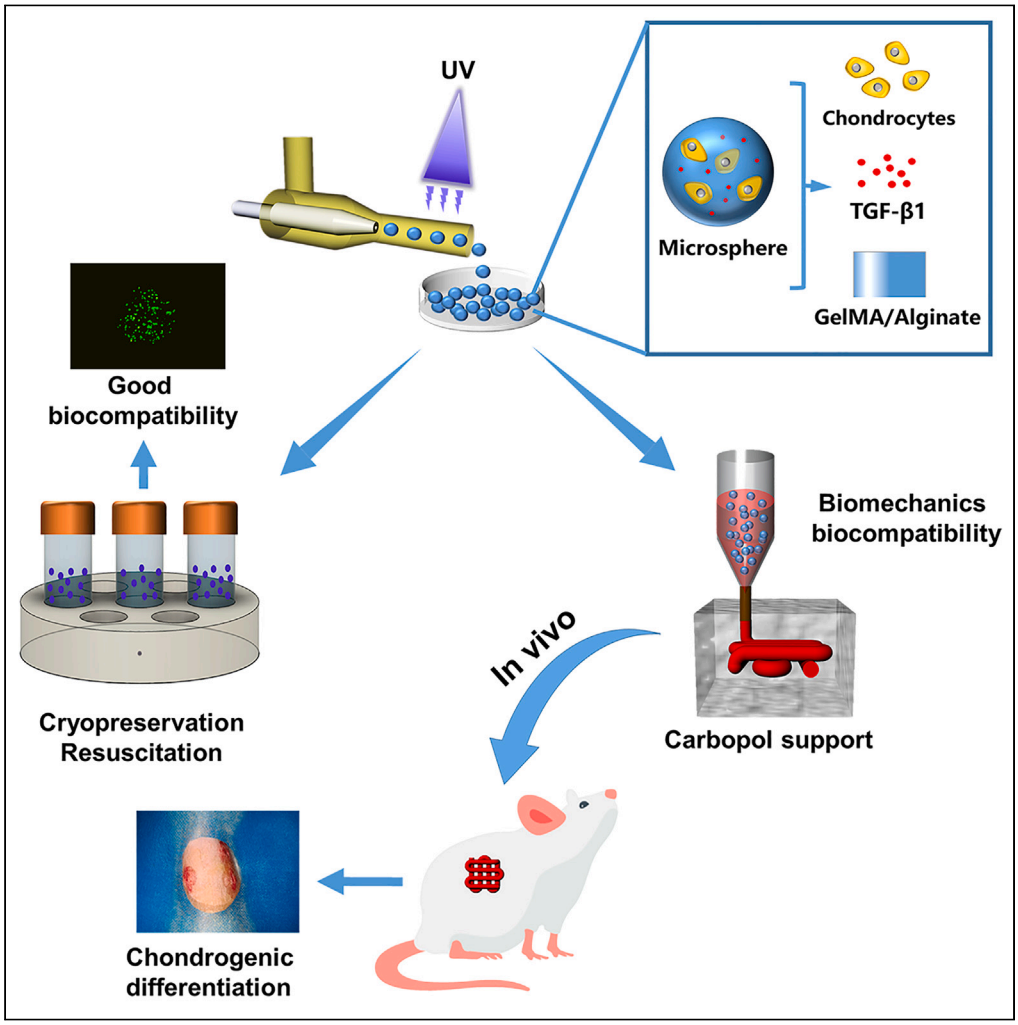

Panjing Yin, Weiwei Su, Ting Li, ..., Yaobin Wu, Chun Zeng, Wenhua Huang

wuyaobin2018@smu.edu.cn (Y.W.)
zengdavid@126.com (C.Z.)
huangwenhua2009@139.com (W.H.)

Highlights

The cells embedded in GA-MS remained viable even after being frozen and resuscitated

A composited hydrogel-based bioinks containing cell-encapsulated GA-MS was prepared

3D printed composited hydrogel-based multiscale scaffold can mimic native cartilage

The 3D printed multiscale scaffolds could be enhancing cartilage repairing *in vivo*

Yin et al., iScience 26, 107349
August 18, 2023
https://doi.org/10.1016/j.isci.2023.107349

iScience

CellPress
OPEN ACCESS

Article

A modular hydrogel bioink containing microsphere-embedded chondrocytes for 3D-printed multiscale composite scaffolds for cartilage repair

Panjing Yin,[1,2,7] Weiwei Su,[2,7] Ting Li,[2,7] Ling Wang,[5] Jianying Pan,[1] Xiaoqi Wu,[2] Yan Shao,[1] Huabin Chen,[1] Lin Lin,[1] Yang Yang,[2] Xiulin Cheng,[6] Yanbing Li,[2] Yaobin Wu,[2,8,*] Chun Zeng,[1,*] and Wenhua Huang[2,3,4,*]

SUMMARY

Articular cartilage tissue engineering is being considered an alternative treatment strategy for promoting cartilage damage repair. Herein, we proposed a modular hydrogel-based bioink containing microsphere-embedded chondrocytes for 3D printing multiscale scaffolds integrating the micro and macro environment of the native articular cartilage. Gelatin methacryloyl (GelMA)/alginate microsphere was prepared by a microfluidic approach, and the chondrocytes embedded in the microspheres remained viable after being frozen and resuscitated. The modular hydrogel bioink could be printed via the gel-in-gel 3D bioprinting strategy for fabricating the multiscale hydrogel-based scaffolds. Meanwhile, the cells cultured in the scaffolds showed good proliferation and differentiation. Furthermore, we also found that the composite hydrogel was biocompatible *in vivo*. These results indicated that the modular hydrogel-based bioinks containing microsphere-embedded chondrocytes for 3D printing multiscale scaffolds could provide a 3D multiscale environment for enhancing cartilage repairing, which would be encouraging considering the numerous alternative applications in articular cartilage tissue engineering.

INTRODUCTION

Common causes of knee cartilage defects are trauma and degenerative diseases, which can result in secondary osteoarthritis.[1,2] Although surgical treatment has improved in recent years, complications and failures still occur.[3,4] Recently, tissue engineering has become a potential therapeutic method for repairing cartilage defects.[5,6] Knee cartilage tissue is hyaline cartilage composed of chondrocytes embedded in a matrix, and most chondrocytes are present in the lacunae of the cartilage in the form of aggregates.[7] However, reported tissue engineering scaffolds for cartilage repair cannot replicate or restore the physiological and anatomical characteristics of the cartilage.[8,9] In particular, the 3D distribution of chondrocytes in the cartilage matrix is not reproduced in cartilage repaired using scaffolds prepared by electrospinning or those containing microspheres. This difference from native cartilage can result in further damage to the articular cartilage because of uneven pressure on the joints. To date, tissue engineering scaffolds that mimic the anatomical characteristics of articular cartilage, which would be more appropriate for cartilage repair, have rarely been reported. Therefore, the fabrication of a multiscale composite scaffold that mimics the 3D complex structure of cartilage tissue for cartilage regeneration remains a great challenge.

Over the past few years, hydrogel-based 3D bioprinting has become a promising technology for cartilage tissue engineering.[10] Recently, a human chondrocyte-laden gelatin meth acryloyl bioink was used for 3D bioprinting with a physical crosslinking method that yielded a simulated cartilage scaffold.[11] However, the hydrogel bioink was prepared by directly mixing cells and hydrogel; thus, the cells were vulnerable to damage induced by shear forces during 3D bioprinting. In addition, the chondrocytes had a scattered distribution in the hydrogel, which does not reflect the physiological distribution of chondrocytes in cartilage lacunae, that is, as aggregates. In contrast, modular bioink is more conducive to the preparation of multiscale composite scaffolds to mimic the 3D micro and macro environment of cartilage tissue.

[1]Department of Joint Surgery, The Third Affiliated Hospital, Southern Medical University, Guangzhou 510630, P.R.China

[2]Guangdong Engineering Research Center for Translation of Medical 3D Printing Application, Guangdong Provincial Key Laboratory of Digital Medicine and Biomechanics, National Key Discipline of Human Anatomy, School of Basic Medical Sciences, Southern Medical University, Guangzhou 510515, China

[3]Guangdong Medical Innovation Platform for Translation of 3D Printing Application, The Third Affiliated Hospital of Southern Medical University, Guangzhou 510000, China

[4]Orthopaedic Center, Affiliated Hospital of Guangdong Medical University, Guangdong Medical University, Zhanjiang 524001, China

[5]School of Biomedical Engineering, Southern Medical University, Guangzhou 510515, Guangdong Province, China

[6]The School of Basic Medical Sciences, Fujian Medical University, Fuzhou 350108, Fujian Province, China

[7]These authors contributed equally

[8]Lead contact

*Correspondence: wuyaobin2018@smu.edu.cn (Y.W.), zengdavid@126.com (C.Z.), huangwenhua2009@139.com (W.H.)

https://doi.org/10.1016/j.isci.2023.107349

Recently, microspheres have also drawn attention for use in cartilage tissue engineering because of their small size, ability to carry drugs and cells, and the modular design of their building blocks.[9,12,13] However, the number of cell-encapsulating microspheres prepared in each microsphere batch is too low for the preparation of multiscale composite scaffolds.[13] Therefore, based on previous research on modular inks,[14–16] we adopted a tissue engineering strategy combining 3D bioprinting and microfluidic technology to develop a suitable multiscale composite hydrogel scaffold. Specifically, chondrocytes were encapsulated in microspheres and mixed with a hydrogel for use as bioinks for 3D bioprinting to prepare a composite scaffold. Crucially, the scaffold can not only protect the chondrocytes in the microspheres from the shear forces during printing, but also simplifies the tedious steps of scaffold preparation to reduce the probability of contamination. Further, concerning the composite scaffold, the microspheres encapsulating chondrocytes mimic the cartilage lacunae and the hydrogel around the microspheres mimics the cartilage matrix at the microscopic level, which can provide a more biomimetic 3D structural environment of chondrocytes to promote better growth and proliferation of chondrocytes. In addition, the overall composite scaffold mimics the structure of cartilage layer at the macroscopic level, which can be fabricated by a 3D printer to fill irregular cartilage defects well. Therefore, the resulting composite scaffold mimics the physiological and anatomical features of cartilage. However, modular bioinks are inconvenient to use because they must be used immediately after preparation, and the production processes are often time-consuming and cumbersome. In addition, as mentioned, the number of cell-encapsulating microspheres prepared in a single batch is too low for the preparation of multiscale composite scaffolds. Burdick et al. reported that microgels could be embedded in granular hydrogels to enable the fabrication of 3D constructs via 3D printing and ejection from syringes.[13] They prepared microgels by vacuum-driven filtration to create granular hydrogels, which required a large number of microspheres. However, the cell-encapsulating microspheres must be protected in an appropriate environment to ensure high cell survival rates. Thus, it is important to design a more convenient and more efficient strategy in cartilage tissue engineering for repairing cartilage defects.

In this study, we present the multiscale composite scaffolds prepared from cryopreserved and subsequently reactivated microspheres mixed with gelatin/methacrylate (GelMA)/alginate hydrogels as bioinks (Figure 1). The double cross-linked network hydrogel (GelMA/alginate) has good biocompatibility and biomechanical properties.[17] The microspheres were prepared by mixing chondrocytes with a GelMA/alginate precursor solution containing aqueous tissue growth factor (TGF-β1) using multichannel microfluidic chips. Subsequently, the microspheres prepared in each batch were frozen and stored in liquid nitrogen at −80°C for later use. When the quantity of microspheres was sufficiently high for the preparation of the scaffold, they were reactivated and mixed into a hydrogel to yield the multiscale bioink, which was extruded-printed into a Carbopol support bath. Subsequently, *in-vitro* cell viability and proliferation assays, immunofluorescence (IF) staining, and *in-vivo* ectopic (subcutaneous) chondrogenesis experiments were performed to show that the composite scaffold is biocompatible and promotes chondrogenic differentiation. Collectively, we believe that the multiscale composite scaffold has great prospects for the clinical repair of cartilage defects.

RESULTS AND DISCUSSION

Preparation and characterization of GA hydrogel

In this study, a double-cross-linked network hydrogel comprising GelMA and alginate was found to show better performance than a single hydrogel. Recent research has shown that the GelMA hydrogel has good biocompatibility and biodegradability, and the preparation of a dual GelMA/alginate hydrogel can result in further improvements in the biomechanical properties compared to those of the GelMA hydrogel.[18–20] Therefore, to date, GelMA/alginate hydrogels have been commonly used for tissue engineering applications.

A schematic of the preparation of the GA hydrogel is shown in Figure S2. In the first step, gelatin was reacted with MA to obtain GelMA, which was then cross-linked by UV light after mixing with LAP. In the second step, alginate cross-linking was achieved by immersion in a calcium chloride solution, thus yielding the hydrogel. A key step in the preparation of GelMA is the binding of the methacrylate groups to the primary amine groups of gelatin.[21] In addition, it is well known that alginate forms a strong ionotropic hydrogel in the presence of divalent cations such as Ca^{2+}. This complexation with Ca^{2+} results in the unique "egg-box" structure.[22] These two steps for the preparation of the double cross-linked hydrogel gelling process are shown in Figure 2A. ^{1}H-NMR analysis of the reaction solution obtained after gelatin had reacted with

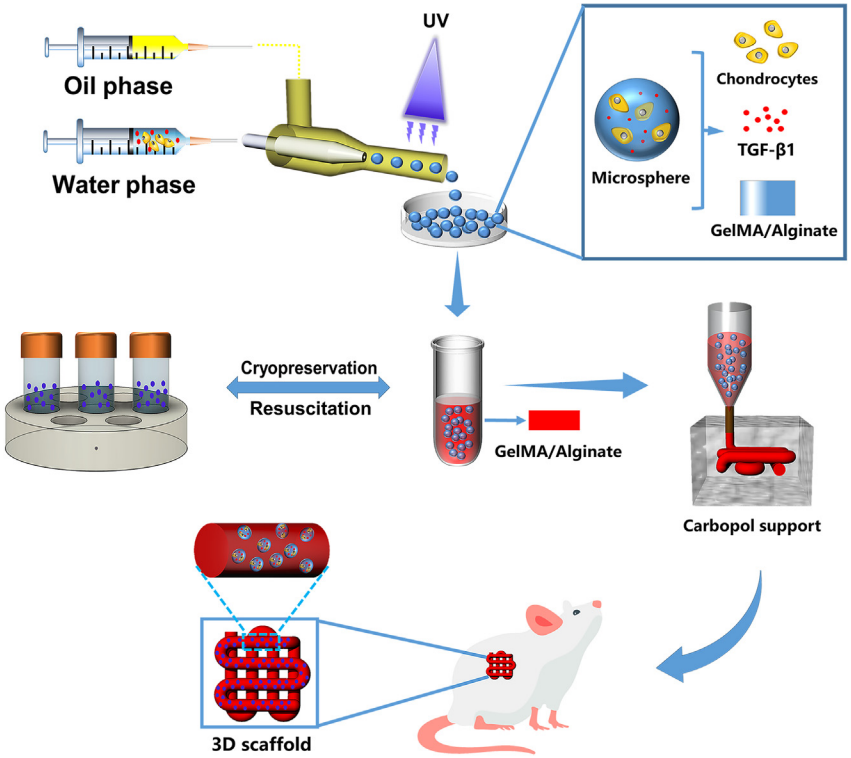

Figure 1. Schematic diagram of the study design chondrocytes, TGF-β1, and GelMA/alginate were mixed as an aqueous-phase solution to prepare cell-encapsulating GA-MS via a microfluidic chip

The cell-encapsulating GA-MS were cryopreserved, resuscitated, and mixed with GelMA/alginate as multiscale bioink, which was then extruded into Carbopol support via a 3D printer to prepare multiscale composite scaffold. The scaffold was then implanted into the subcutaneous tissue of the mice.

MA revealed that the intensities of the signals related to the methacrylamide vinyl group at 5.4 and 5.6 ppm increased significantly; these signals correspond to the two protons in the methacrylate double bonds (Figure S1A), indicating that gelatin had been successfully modified with MA. In addition, bands characteristic of the functional groups in GelMA and alginate were observed in the FT-IR spectra of GelMA/alginate, as shown in Figure S1B. In particular, the bands around 3325 and 1680 cm^{-1} correspond to the –OH groups and C=C bonds, respectively, of the GelMA hydrogel. In addition, the bands at 1624 and 1432 cm^{-1} correspond to the antisymmetric and symmetric stretching vibrations of the –COOH groups in the alginate hydrogel. These results indicate that GelMA and alginate were well mixed. The degree of substitution of GelMA was 94%, as calculated using the ninhydrin reaction (Table S1).

The swelling properties of the GA hydrogels were investigated using different concentrations of GelMA (5%, 10%, and 15% w/v) while the amount of alginate was kept constant (1.2% w/v). In these experiments, the lyophilized hydrogels were immersed in PBS and weighed every 5 min for 40 min, as shown in Figure 2B. The swelling rate was most rapid in the first 5 min after immersion in PBS and rapidly reached equilibrium. Furthermore, with an increase in GelMA concentration, the degree of swelling gradually increased. The degradation rates and shear viscosities of these hydrogels are shown in Figure 2B. Notably, the degradation rate of the 15% (w/v) GA hydrogel was lower than that of the 5% (w/v) GA hydrogel. In addition, all three GA hydrogels exhibited shear thinning behavior, indicating their suitability for printing. In particular, with increasing GA hydrogel concentration, the shear viscosity gradually increased.

To select the appropriate mechanical properties of hydrogel, a double crosslinking network hydrogel (that is, the GA hydrogel) was used to prepare microspheres instead of a single hydrogel. As shown in Figures 2C–2E, the storage modulus (G') of the GA hydrogel was higher than that of the single-component GelMA and alginate hydrogels, and the storage modulus (G') was always higher than the loss modulus (G'') in the observed range of shear rates. Specifically, the storage modulus (G') of the double cross-linked

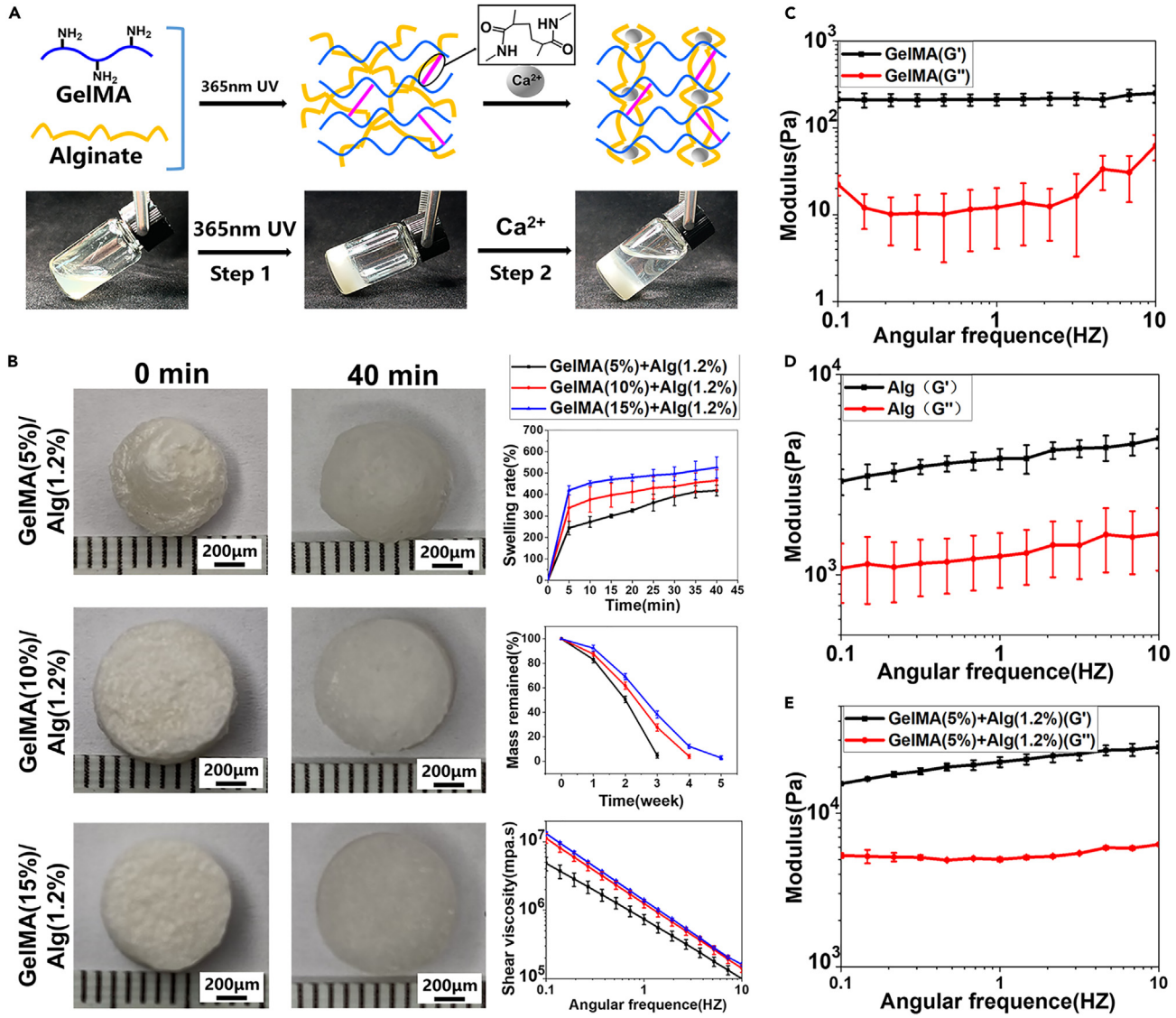

Figure 2. Characterization and preparation of GelMA and alginate hydrogel (n = 4, n represents number of hydrogel samples)

(A) Gelation process of GA double cross-linking network hydrogel after photo-crosslinking and physical-crosslinking.

(B) Swelling property, remaining mass, and shear viscosity of the different concentrations of GA hydrogels including GelMA (5%, 10%, and 15% w/v)/alginate (1.2% w/v).

(C–E) Storage modulus (*G'*) and loss modulus (*G''*) of GelMA, alginate, and GA hydrogel in the angular frequency ranging from 0.1 to 10 rad/s.

network hydrogel (GelMA/alginate) was in the range of 15 ± 0.2–27 ± 2.3 Kpa. One study has determined the storage modulus required for chondrogenesis to be in the range of 7–33 Kpa,[23] which indicated that the GelMA/alginate hydrogel we selected was suitable for the growth of chondrocytes. In addition, several studies have shown that mechanical forces have a significant effect on cell growth.[24,25] Therefore, materials with appropriate modulus are of great significance for the growth of chondrocytes. These results indicate that the addition of alginate improves the biomechanical properties of GelMA, and that the GA hydrogel was sufficiently stable to maintain gelatinous behavior on the application of shear. The SEM images of the freeze-dried GelMA hydrogels are shown in Figure S3. From these images, it was found that the pore size of the hydrogels decreased with an increase in GelMA concentration. In particular, the pores of the 5% (w/v) GelMA hydrogel were significantly larger than those in the other two samples. These large pores are beneficial for the encapsulation of chondrocytes. In addition, the porosity of GelMA decreased with increase in the GelMA concentration.

Preparation of microspheres based on a multichannel microfluidic chip

There are many methods for the preparation of microspheres, including the use of microfluidic emulsions, lithography, electrohydrodynamics, and mechanical fragmentation.[26–29] Compared with other methods, the use of microfluidic chips allows the production of large numbers of uniformly sized microspheres. The principle behind this technique is as follows: At the point of contact between the water and oil phases in the microfluidic chip, the water phase is subjected to shear forces, as well as hydrophobic interactions with the oil phase, thus resulting in the formation of microspheres.[30] However, traditional capillary microfluidic chips require complex fabrication processes and have short service lives because the internal channels are easily blocked.[31] In this study, we designed a multichannel microfluidic chip composed of two inlets, one outlet, and five parallel internal phase channels, which allowed us to obtain a high microsphere yield and long chip life. The channels and an overall chip schematic are shown in Figure 3A (I–IV). The five parallel channels are identical and remained unobstructed during use. A design diagram of the chip is given in Figures S4A–S4D. The lengths of the inlets (F and G) and outlet (H) were 6 mm. The inner and outer diameters of the inlets (F, G) were 1.0 and 2.5 mm, respectively, the inner and outer diameters of the outlet (H) were 1.5 and 3.0 mm, respectively, and the inner and outer diameters of the internal phase channel outlet (I) were 0.1 and 0.3 mm, respectively. The main body of the chip was 15 mm long, 14.25 mm wide, and 7.25 mm high. Three views of the chip and the moment when the microspheres exited the inner phase channel of the chip are shown in Figure 3B (I–IV). As shown, the chip can produce a large number of homogeneous microspheres.

In this study, 5% GelMA, 1.2% alginate, and GelMA (5%)/alginate (1.2%) were used as the water phase to prepare microspheres (MS) with the same settings as other conditions. The diameters of the prepared microspheres were 445 $\pm$ 5, 399 $\pm$ 8, and 366 $\pm$ 4 μm, as shown in Figures S5A–S5D. The small size of the GA-MS (GelMA /alginate microspheres) further shows that the double-crosslinking network material is more stable than the single-component materials. Therefore, the double crosslinking network material (GelMA/alginate, GA) was selected to prepare GA-MS. In fact, the relative flow rates of the water and oil phase solutions significantly affected the diameter and uniformity of the formed GA-MS (Figure 3C (I–VII). As shown in Figure 3C (VIII) and Table S1, when the flow rate of the water phase was 10 μL/min and the flow rate of the oil phase was increased (300, 600, 900, 1200, and 1500 μL/min), the diameters of the GA-MS were inversely proportional to the oil-phase flow rate. In contrast, when the flow rate of the oil-phase was 900 μL/min and the flow rate of the water phase was increased (5, 10, and 15 μL/min), the diameters of GA-MS were proportional to the flow rate of the water phase. To encapsulate sufficient chondrocytes in the GA-MS, as well as provide sufficient nutrients, GA-MS having a diameter of 88 $\pm$ 5 μm were selected. As shown in Figure 3D, the prepared GA-MS were uniform in size, and their surfaces were smooth. Thus, homogeneous microspheres could be prepared in large quantities using the multichannel microfluidic chip, and microspheres with different diameters could be prepared by changing the flow rate of the working solution.

Sustained release of BSA-FITC and BSA within GA-MS

Recently, microspheres have become popular for the sustained release of nutritional components and drugs.[32] In this study, microspheres were prepared using microfluidic chips, and their sustained-release properties were analyzed qualitatively and quantitatively. In one experiment, GA-MS containing Bovine serum albumin-Fluorescein isothiocyanate (BSA-FITC) was immersed in Dulbecco's buffered saline (DPBS) to observe its sustained release. Then, fluorescence microscopy images were obtained after 0, 3, 9, 21, and 36 h (Figure 4A). As shown, the fluorescence intensity decreased with an increase in immersion time, suggesting good sustained-release ability. Furthermore, the fluorescence signals in the periphery of the GA-MS containing BSA-FITC from 3 to 36 h were stronger than those in the center, indicating that BSA-FITC diffused more rapidly from the core than from the periphery. A possible reason for this is that the pores inside GA-MS are larger than those on the surface.[33] In Figure 4B, the fluorescence microscopy images were converted to an interactive 3D surface plot, showing that the height of the gray level of the 3D plot decreased with time. In addition, the peak of the gray level of the data matrix frequency also shifted to a lower value over time (Figure 4C). These results indicate that the BSA-FITC contained inside the GA-MS was released over a sustained period. Further, the means and standard deviations of the gray levels also decreased with time, as shown in Figures 4D and 4E, indicating that BSA-FITC underwent sustained release from the interior of the GA-MS. In another experiment, GA-MS with different diameters containing BSA were immersed in DPBS to explore the effect of diameter on the release behavior of GA-MS. As shown in Figure 4F, the GA-MS having diameters of 246 $\pm$ 6 μm had the fastest sustained release rate, and those

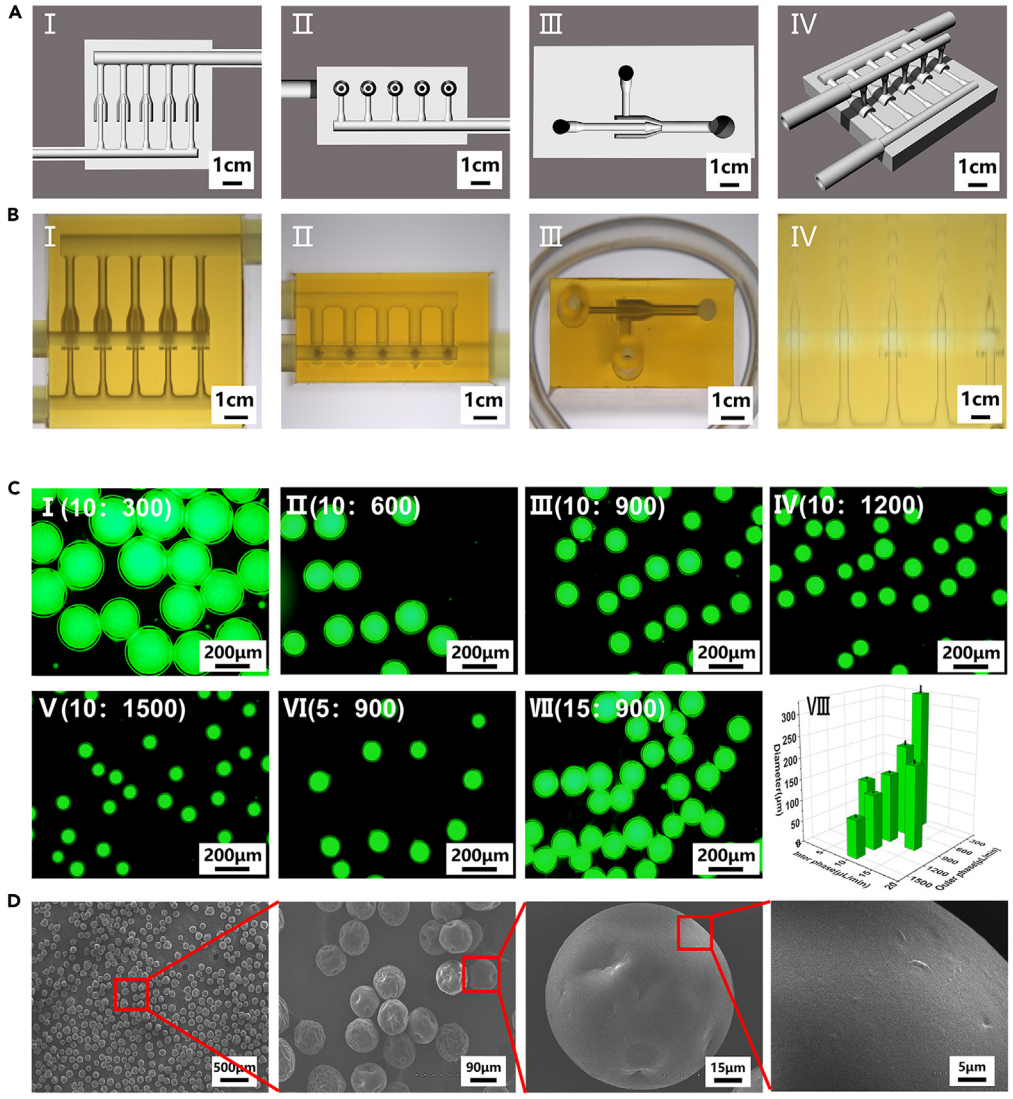

Figure 3. Characterization of the microfluidic chip and microspheres

(A) Schematic diagram of the microfluidic chip model used here. Cross-sectional schematic diagram of the chip in three views(I–III) and the overall schematic diagram of the chip (IV).

(B) Three views of the microfluidic chip (I–III) and the moment when microspheres exit from the inner phase channel of the chip (IV).

(C) Morphological analysis of GA-MS with different diameters (n = 3, n represents number of GA-MS sample groups). FITC-dyeing GA-MS with the same water-phase flow rate but different oil-phase flow rates (I–V) and FITC-dyeing GA-MS with the same oil-phase flow rate but different water-phase flow rates (III, VI, VII). The statistical diagram of microsphere diameters (VIII).

(D) SEM images of GA-MS that show their dispersed homogeneous morphologies.

having diameters of 457 ± 3 μm had the slowest release rate. After 3 h, the optical density (OD) values of the GA-MS having diameters of 246 ± 6, 361 ± 4, and 457 ± 3 μm were 0.254 ± 0.011, 0.172 ± 0.006, and 0.133 ± 0.002, respectively. Thus, the release rate was inversely proportional to the diameter of the GA-MS. These results indicate that the GA-MS prepared using our microfluidic chips have a great potential for facilitating a sustained release of nutrients and drugs.

Biological assessment of the GelMA hydrogel and GA-MS

GelMA-based hydrogels are widely used for cartilage tissue engineering.[34] Notably, the concentration of the GelMA hydrogel affects the ability of the cells encapsulated in the hydrogel to spread.[35] As shown in

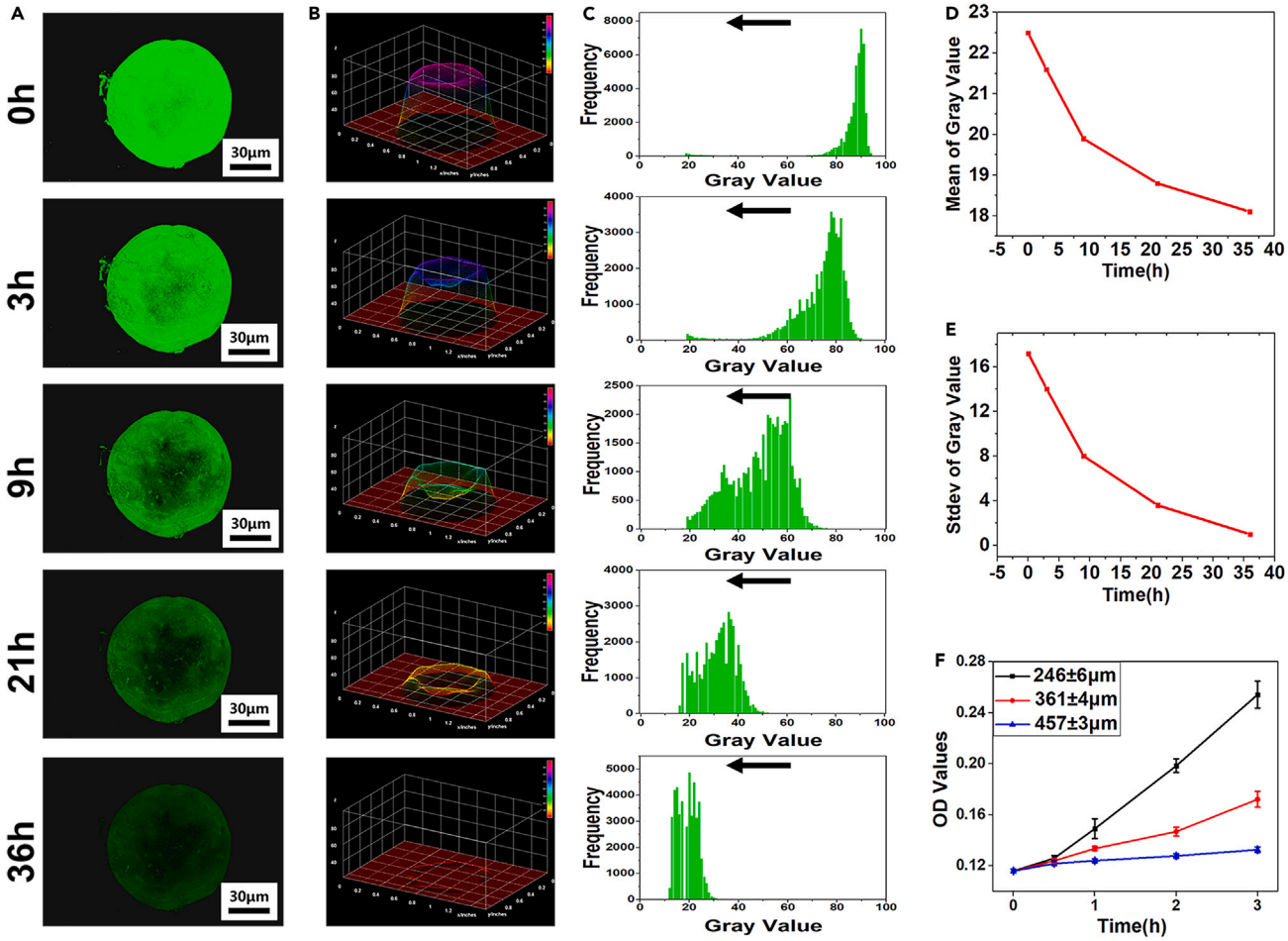

Figure 4. Analysis of sustained release of BSA-FITC loaded inside GA-MS (n = 3, n represents number of GA-MS sample groups)

(A) Confocal fluorescence microscopy images of GA-MS containing BSA-FITC. The fluorescence intensity of images decreased with the extension of immersing time.

(B) Fluorescence microscopy images converted to interactive 3D surface plots.

(C) Distribution histograms of gray value distribution of interactive 3D surface plot converted from confocal microscopy images.

(D and E) Means and standard deviations of the gray levels after 0, 3, 9, 21, and 36 h.

(F) Cumulative release of BSA for the 457 ± 3, 361 ± 4, and 246 ± 6 μm particles of GA-MS after 0.5, 1, 2, and 3 h of immersion in DPBS.

Figure S6, the area over which the chondrocytes spread decreased with an increase in GelMA concentration. In particular, the area over which the chondrocytes spread was highest for the 5% (w/v) GelMA hydrogel (compared with the 10% and 15% (w/v) GelMA hydrogels), possibly as a result of the differences in the pore sizes of the freeze-dried GelMA hydrogels. Specifically, the pores were larger at low concentrations of GelMA than high concentrations, and the larger pore sizes resulted in a greater spreading area of the encapsulated chondrocytes. Therefore, considering the biocompatibility and mechanical properties of the GelMA (5% w/v)/alginate (1.2% w/v) hydrogel, this was selected to prepare microspheres for use in the tissue engineering scaffolds.

Compared with the traditional culture method in which cells are loaded on the surface of microspheres, encapsulation in microspheres better simulates the three-dimensional environment of cartilage, which could enhance cell survival. In particular, the 3D distribution of cells allows a higher cell loading than surface loading. The preparation of the chondrocyte-encapsulating GA-MS is shown in Figure S7 and Video S1. To investigate the effects of cryopreservation on the physiological function and survival of chondrocytes encapsulated in GA-MS, the GA-MS containing chondrocytes were frozen and stored in liquid nitrogen for 7 days and then reactivated for culture (denoted the *frozen group*). Note that these samples were also treated with a cryoprotectant. In addition, GA-MS with chondrocytes that were directly cultured

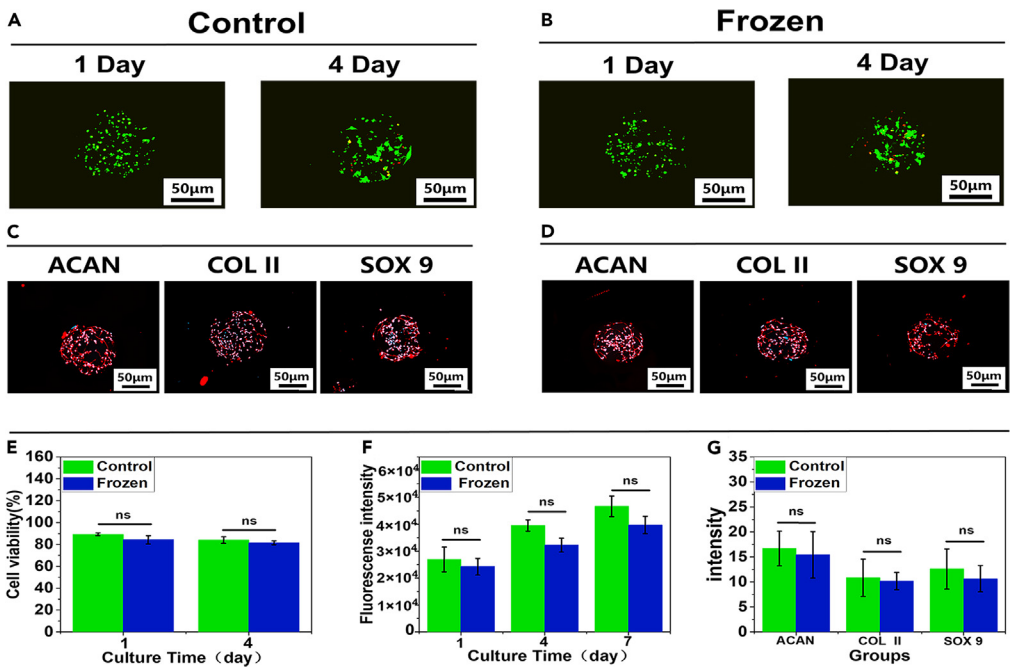

Figure 5. *In-vitro* biological characterization of cell-encapsulated GA-MS (n = 3, n represents number of GA-MS sample groups)

(A and B) Confocal microscopy images of live/dead staining of the chondrocyte-encapsulated GA-MS in the control and frozen groups after culture for 1 and 4 days.

(C and D) Immunofluorescence staining images of the chondrocyte-encapsulated GA-MS in the control and frozen groups after culture for 7 days.

(E–G) Quantitative analysis of cell viability, cell proliferation, and qualitative analysis of extracellular matrix proteins of the chondrocyte-encapsulated GA-MS in the control and frozen groups. "NS" represents no significant difference.

without cryopreservation was used as the *control group*. In addition, both frozen and control groups were treated with TGF-β1 to promote cell proliferation and matrix protein production.[36] Optical microscopy observation revealed that the GA-MS remained intact after reactivation (Figure S8). As shown in Figures 5A, 5B, and 5E, the viabilities of the chondrocytes in both the control and frozen groups were higher than 80% on days 1 and 4. Furthermore, statistical analysis showed that the cell viabilities were as high as 89.4 ± 1.15% (control group) and 84.3 ± 3.79% (frozen group) after 1 day of culture, and 84.1 ± 2.93% (control group), and 81.6 ± 1.69% (frozen group) after 4 days of culture. No significant differences were observed between the control and the frozen groups. In addition, fluorescence analysis of both groups after 1, 4, and 7 days of culture (Figure 5F) showed that the fluorescence intensity of the two groups increased gradually, and there were no significant differences between the two groups. The above results indicate that the GA-MS protected the chondrocytes from the effects of cryopreservation and reactivation compared to the control group. In addition, in both groups, the chondrocytes were evenly distributed inside the microspheres after 1 day of culture, whereas some of the chondrocytes gradually transferred to the outer layer of the GA-MS and appeared to aggregate after 4 days of culture. This can be explained as follows: In biological and pathological processes, cells migrate from areas of low oxygen concentrations to areas of optimal oxygen concentration, which is known as "aerotaxis".[37] Generally, hydrogel microspheres allow the diffusion of nutrients and oxygen,[38] although the outer layer of the microspheres is likely to experience greater oxygen diffusion. In addition, the chondrocytes in the GA-MS aggregate because of the secretion of matrix proteins, including ACAN, COL II, and SOX9, which promote inter-cell interactions and aggregation.[39] As shown in Figures 5C and 5D, the IF staining results indicate that chondrocytes in GA-MS in both groups deposited a large number of matrix proteins, including ACAN, COL II, and SOX9, after 7 days of culture. The images of IF staining were semi-quantitatively analyzed, which was shown in Figure 5G. There was no significant difference between the two groups, indicating that cryopreservation and reactivation did not affect protein expression. A possible explanation for this result is that the cryoprotectant infiltrated the GA-MS and penetrated the chondrocytes, thus providing protection. Moreover, the matrix proteins protect chondrocytes from damage during cryopreservation.[40]

To produce sufficient numbers of chondrocyte-encapsulating GA-MS for 3D bioprinting and reduce the risk of contamination, cryopreservation in liquid nitrogen until use is necessary, and our results indicate that the encapsulation of these cells in the microspheres had a good cell-protecting effect. Notably, these microspheres have also been used in the field of cell preservation.[40] Based on our findings, we believe that these microspheres will aid the development of 3D bioprinting combined with microfluidic technology for cartilage tissue engineering.

Construction of 3D multiscale composite scaffolds in a Carbopol support bath

Soft hydrogel materials often collapse under their own weight during direct ink writing (DIW); however, the gel-in-gel printing technique can solve this problem.[41] Therefore, Carbopol hydrogel was used because of its good supporting effects. Images of the Carbopol support baths having different concentrations (0.2%, 0.7%, and 1.2% w/v) after bubble removal, as well as the results of shear testing, are shown in Figure S9A. As the Carbopol concentration increased, the transparency of the Carbopol support bath decreased gradually, whereas the shear viscosity increased. Therefore, considering the need for a good supporting bath, a Carbopol solution having a concentration of 0.7% w/v was selected. During the printing process, many different parameters, including temperature, extrusion pressure, printing speed, and needle diameter, affect the diameter of the printed wire.[42] By varying one printing parameter while keeping the others constant, we found that the temperature and extrusion pressure were directly proportional to the diameter of the printing wire, whereas the printing speed and needle diameter were inversely proportional to the diameter of the printing wire (Figure S9B). In particular, it was found that when the temperature was lowered to 14°C, the printing wire had an uneven thickness, possibly because the hydrogel ink gel was harder to extrude at such low temperatures. Of all the investigated parameters, the needle diameter had the most significant effect on the diameter of the printed wire. After experimentation, the optimal conditions were found to be a temperature of 21°C, extrusion pressure of 3.5 bar, the printing speed of 8.0 mm/s, and needle diameter of 22G; these conditions yielded a straight and homogeneously thick printed wire. As shown in Figure S10A, circles and pentagons could be printed perfectly under these conditions, demonstrating the high accuracy and sensitivity of printing in the Carbopol support bath.

In traditional 3D bioink printing methods, the hydrogel is directly mixed with cells as bioink for preparing scaffolds.[43] However, the inconvenience and low cell viability after transplantation via the traditional methods have limited chondrocyte utilization. On the one hand, traditional bioink preparation is time-consuming and cumbersome, and, crucially, there is a significant risk of contamination because the cells must be cultured and sub-cultured to achieve a sufficient number, followed by digestion and mixing with the hydrogel. On the other hand, the cells were vulnerable to damage induced by shear forces during 3D bioprinting. In addition, the chondrocytes had a scattered distribution in the hydrogel, which does not reflect the physiological distribution of chondrocytes in cartilage lacunae; that is, as aggregates. In this study, we present the multiscale composite scaffolds prepared from cryopreserved and subsequently reactivated microspheres mixed with gelatin/methacrylate (GelMA)/alginate hydrogels as bioinks. To produce a sufficient number of chondrocyte-encapsulating GA-MS for printing, batch production was carried out, and the produced microspheres were cryopreserved in liquid nitrogen. Subsequently, to produce the multiscale composite scaffolds, the chondrocyte-encapsulating GA-MS were thawed and reactivated and then mixed in the GelMA/alginate hydrogel to form a multifunctional modular bioink, denoted as GA-MS/GM-alg (see Figure S10B and Video S2 for details of the preparation process). SEM images of the multiscale composite scaffolds are shown in Figure 6A. Notably, the surfaces of the scaffolds after lyophilization are not smooth, which could be a result of water loss, indicating that scaffolds should be used as soon as possible after preparation. To observe the distribution of GA-MS in the composite scaffolds, the GA-MS was dyed green with FITC, and the GelMA/alginate precursor solution was dyed red with rhodamine. Macroscopic images of the composite scaffolds are shown in Figure 6B (I–IV), revealing that the GA-MS were uniformly distributed in the composite scaffolds. Further, the composite scaffolds were loaded with a large number of GA-MS which, correspondingly, resulted in the loading of the scaffolds with a large number of chondrocytes. Microscopic images of the composite scaffolds are shown in Figure 6C I and reveal that the GA-MS were uniformly distributed throughout the composite scaffold. Figure 6C II shows an interactive 3D surface plot converted from Figure 6C I, showing the same result. Based on these results, the multifunctional GA-MS/GM-alg modular bioink is deemed suitable for the production of multiscale composite scaffolds.

Anatomically, human knee cartilage is hyaline cartilage containing chondrocytes and a surrounding matrix, and most of the chondrocytes are present as aggregates in the cartilage lacunae. To explore the effect of

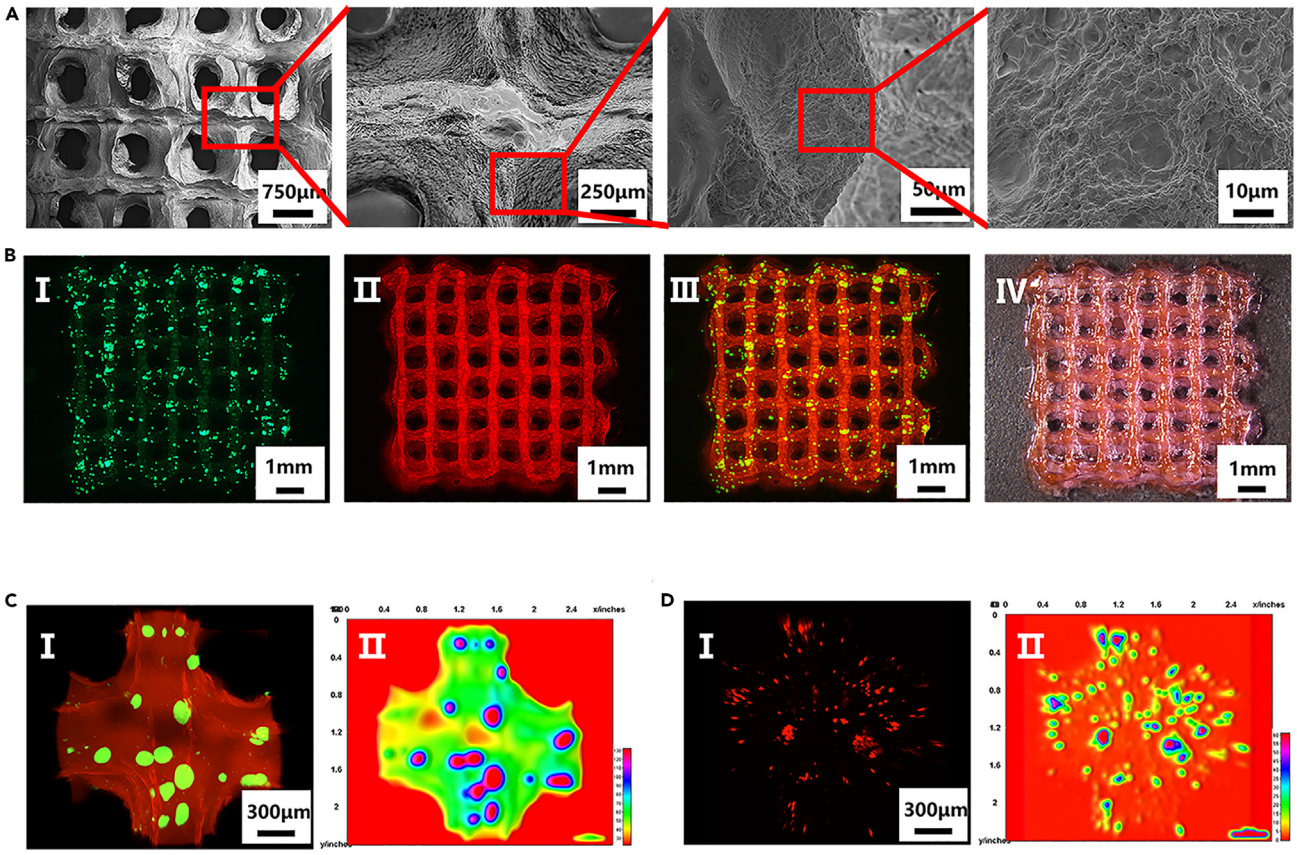

Figure 6. Characterization of the multiscale composite scaffolds

(A) Scanning electron microscopy images of the composite scaffolds.

(B) Fluorescence (I–III) and white light (IV) stereomicroscopic images of the composite scaffolds. GA-MS was stained green by FITC and GM-alg was stained red by rhodamine.

(C and D) Confocal fluorescence microscopy images of the GA-MS/GM-alg composite scaffolds. GA-MS was stained with FITC and GM-alg was stained with rhodamine (C I). Chondrocytes encapsulated in GA-MS within the scaffolds were labeled with Cell Tracker Red CMTPX Dye (D I). Interactive 3D surface plots (C II, D II) were converted from confocal fluorescence microscopy images (C I, D I).

embedding the chondrocytes in the GA-MS and the composite scaffolds, the chondrocyte membrane was labeled with Cell Tracker Red CMTPX Dye. As shown in Figure 6D I, the confocal microscopy images reveal that a small number of GA-MS-encapsulated chondrocytes had been broken by the extrusion forces during printing, causing chondrocytes inside the GA-MS to be dispersed in the composite scaffolds, thus mimicking the chondrocytes scattered on the surface of knee cartilage. However, most of the encapsulated chondrocytes were intact and aggregated, as observed in knee cartilage lacunae. Figure 6D II shows an interactive 3D surface plot converted from Figure 6D I, which shows the distribution of encapsulated chondrocytes in the composite scaffolds more clearly. Based on these results, the multiscale composite scaffolds are promising for applications in clinical cartilage tissue engineering not only because the preparation of the multiscale composite scaffolds was simplified but also because the environment of the scaffold mimics the physiological and anatomical characteristics of human knee cartilage.

Cartilage regeneration experiments

When hydrogel materials, which often have poor hemocompatibility, come into contact with erythrocytes in the blood, the erythrocytes rupture, and the hemoglobin escapes from the cells; that is, hemolysis occurs.[44] An HR value of less than 5% is required for the hydrogels to be used in clinical applications. As shown in Figure S11, no hemolysis was observed in the supernatant of the negative control group (PBS), whereas hemolysis was observed in the positive control group (deionized water). The HR of the three experimental groups were all lower than 5%, and those of the GelMA group and GM-alg group were significantly lower than the alginate group, suggesting that the GM-alg hydrogel has clinical applications.

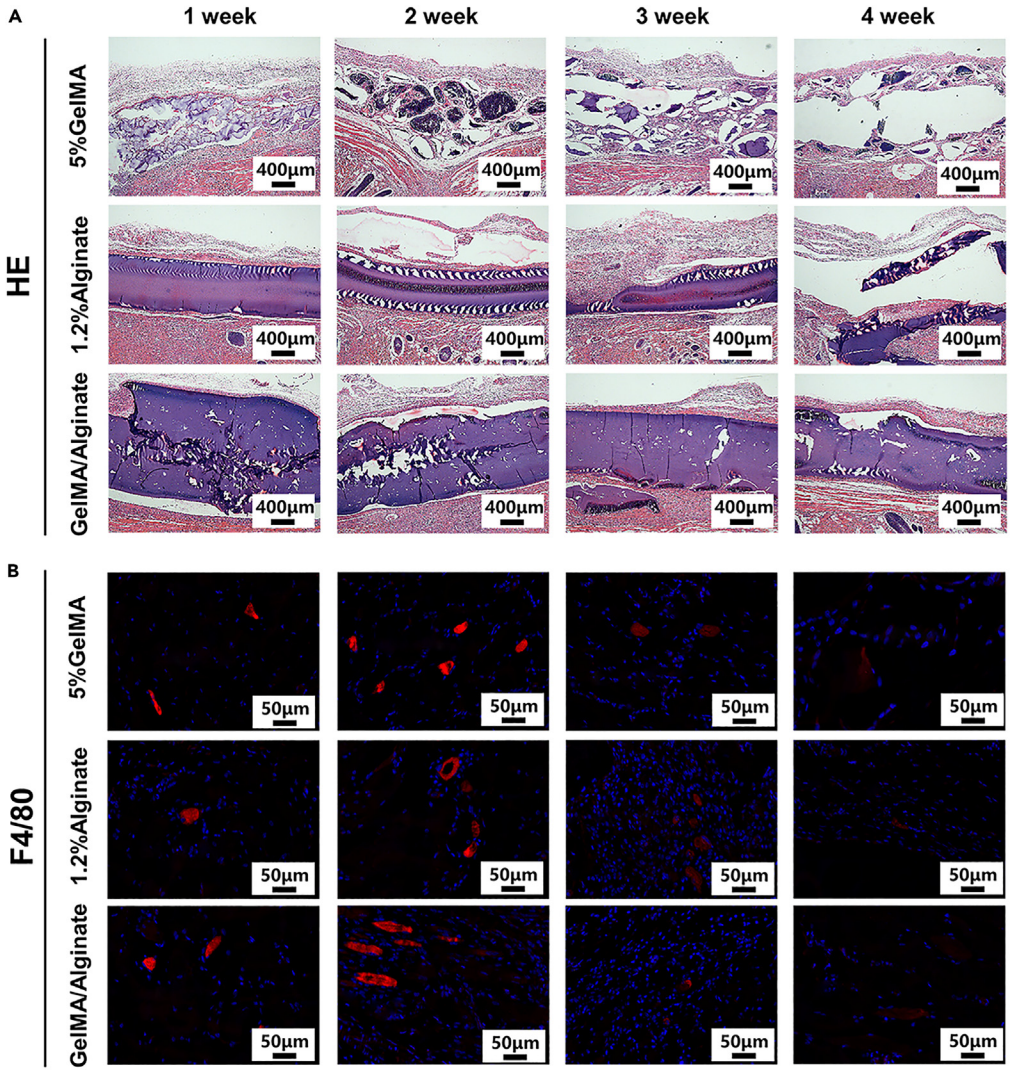

Figure 7. Four SD rats each were implanted with the scaffolds from the three groups, including the GelMA group, alginate group, and GM-alg group, *in vivo*

(A) Scaffolds were retrieved with the surrounding tissue at time points of 1-, 2-, 3-, and 4-week after implantation, which were stained with HE.

(B) F4/80 immunofluorescence sections show macrophages.

In addition, the implantation of scaffolds in animals can induce host reactions, including inflammation and the formation of granulation tissue between the scaffold and tissue.[45] To verify the biocompatibility of the hydrogel materials *in vivo*, scaffolds in each group were implanted in SD rats (Figure S12A). The scaffolds were retrieved with the surrounding tissue after 1-, 2-, 3-, and 4-week post implantation (Figure S12B). As shown in Figure 7A, the sections were treated with HE staining to observe the biocompatibility and degradation of the material *in vivo*. As shown, there was no significant formation of granulation tissue around the subcutaneous scaffolds in either group. In addition, with an increase in implantation time, the alginate group showed a rapid degradation rate, whereas the GM/alg group showed almost no degradation, likely because the GM-alg group was cross-linked twice, which resulted in a dense structure and slow rate of degradation.

Furthermore, since the implantation of foreign materials triggers a recruitment of inflammatory cells (macrophages), a measurement of cell inflammatory responses is a good metric for the biocompatibility of scaffolds. In particular, the implantation of polypropylene and silica gel into the subcutaneous tissue of mice

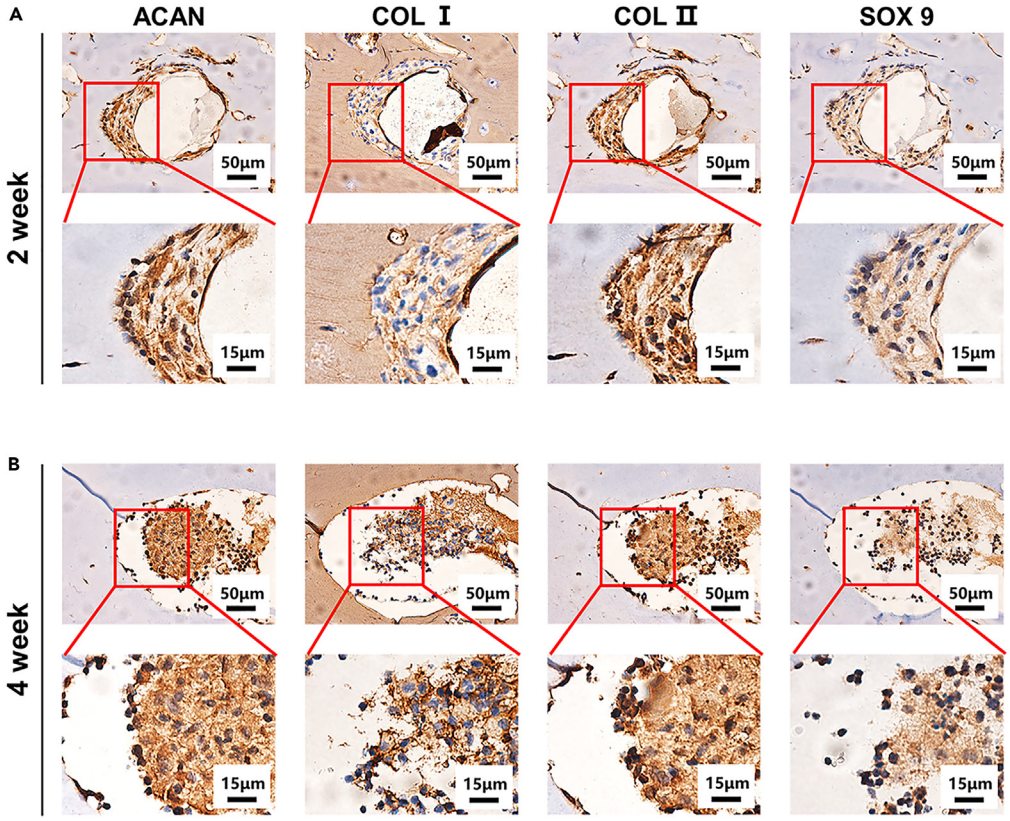

Figure 8. Eight mice each were implanted with the scaffolds containing microsphere-embedded chondrocytes *in vivo*

(A and B) The scaffolds implanted subcutaneously at week 2 A.) and week 4 B) were stained with immunohistochemical staining (ACAN, COL I, COL II, and SOX 9).

has been reported to result in the appearance of macrophages for up to six months, and the number of macrophages increased initially, before subsequently decreasing.[46] In this study, the number of macrophages significantly decreased in all three groups after 3- and 4-week post implantation (Figures 7B and S13). On the basis of these results, the alginate, GelMA, and GM-alg scaffolds have low immunogenicity and good biocompatibility.

Although there are differences in the physiological microenvironment and mechanical load in subcutaneous tissue and joints, the subcutaneous composite scaffolds were still subjected to a certain degree of stress as a result of limb movement extrusion and skin tension.[47] Therefore, the multiscale composite scaffolds were implanted under the skin of the nude mice to simulate the pressure that the scaffolds would experience in the joint cavity. To investigate the chondrogenic ability of the composite scaffolds *in vivo*, cryopreserved GA-MS encapsulating chondrocytes were reactivated and added to the sterile GelMA/alg precursor solution to print scaffolds that were subsequently implanted subcutaneously in nude mice. After implantation, the ability of the chondrocytes to differentiate into cartilage was determined by observing the expression of ACAN, COL I, COL II, and SOX 9 through immunohistochemical staining. As shown in Figure 8, after 2 and 4 weeks, the embedded chondrocytes had deposited ACAN, COL I, COL II, and SOX 9. Moreover, the amounts of ACAN and COL II deposited by the chondrocytes were significantly higher than those of SOX9 and COL I in the second week of scaffold implantation (Figure 8A), indicating that the chondrocytes in the composite scaffolds differentiated into hyaline rather than fibrous cartilage. Four weeks after implantation, the deposition of ACAN, COL I, COL II, and SOX 9 in the chondrocytes increased. There are two possible reasons for the chondrogenic differentiation observed in the composite scaffolds. On the one hand, GelMA and alginate, like the natural cartilage matrix, have good biomechanical properties and biocompatibility. On the other hand, the GA-MS provided a platform for

the chondrocytes to aggregate, which promoted interactions and the enhanced growth of the chondrocytes. These characteristics of the multiscale composite scaffolds make them promising for the treatment of cartilage defects.

Conclusion

In this study, we developed GA-MS containing chondrocytes that could be cryopreserved, reactivated, and mixed with GelMA/alginate precursor solution as a modular bioink. This bioink could then be 3D-printed to yield a multiscale composite scaffold for cartilage tissue regeneration. Notably, the viabilities of the chondrocytes embedded in the GA-MS were retained after cryopreservation and reactivation. Crucially, after implantation, the chondrocytes in the multiscale composite scaffolds differentiated into cartilage, as shown by the secretion of ACAN, COL I, COL II, and SOX 9. This can be explained by the fact that the GA-MS provides a similar environment for the chondrocytes, which are present as aggregates in the lacunae, to that of native cartilage. Further, the GelMA/alginate hydrogel mixed with the GA-MS simulates the surrounding cartilage matrix and shows good biocompatibility and biomechanical properties. Promisingly, the ability to freeze and reactivate the GA-MS containing chondrocytes simplifies scaffold preparation and protects the cells during 3D printing, allowing complex 3D scaffolds that mimic the native environment of chondrocytes to be prepared. This should promote cartilage tissue regeneration. Therefore, the multiscale composite scaffolds have great promise for the clinical treatment of cartilage tissue injury.

Limitations of the study

In this study, the multiscale composite scaffold was fabricated by a 3D printer. The appearance of the scaffold prepared by 3D printing was a traditional grid-like structure, rather than an irregular cartilage defect model constructed by computed tomography. In addition, the multiscale composite scaffold was only implanted subcutaneously in mice, but not implanted in the injured knee joint *in situ*. Therefore, it is still difficult for the biological tissue strategies to be translated into clinical practice. These studies aimed to explore the potential of the multiscale composite scaffold to differentiate into hyaline cartilage, but its ability to repair knee cartilage needs to be further explored.

STAR★METHODS

Detailed methods are provided in the online version of this paper and include the following:

- KEY RESOURCES TABLE
- RESOURCE AVAILABILITY
  - Lead contact
  - Materials availability
  - Data and code availability
- EXPERIMENTAL MODEL AND STUDY PARTICIPANT DETAILS
  - Animals
  - Cell culture
- METHOD DETAILS
  - Preparation and characterization of GelMA and GelMA/alginate (GA) hydrogels
  - Multichannel microfluidic chip design and fabrication
  - Fabrication of GelMA (G-MS), alginate (A-MS), and GelMA/alginate (GA-MS) microspheres
  - Sustained release of BSA-FITC and BSA within GA-MS
  - Spreading ability of chondrocytes in the GelMA hydrogel
  - *In-vitro* biological characterization of cell-encapsulated GA-MS
  - Preparation and rheological property of the Carbopol support bath
  - Composite hydrogel printing based on Carbopol support bath
  - Construction of 3D multiscale composite scaffolds in the Carbopol support bath
  - Hemolysis rate (HR) of materials
  - *In-vivo* investigation of the 3D multiscale composite scaffolds
- QUANTIFICATION AND STATISTICAL ANALYSIS

SUPPLEMENTAL INFORMATION

Supplemental information can be found online at https://doi.org/10.1016/j.isci.2023.107349.

ACKNOWLEDGMENTS

This work was supported by the National Key R&D Program of China(2022YFB4600600), the National Natural Science Foundation of China (31972915, 32271181, 81974327), Guangdong Basic and Applied Basic Research Foundation (2021B1515120019, 2020B1515120001), the Science Natural Foundation of Guangdong province (2022A1515011101), the Science and Technology Project of Guangdong Province(2018B090944002), Discipline construction project of Guangdong Medical University(G622280009 , 4SG22260G).

AUTHOR CONTRIBUTIONS

Y.P.J. (First Author): Conceptualization, Methodology, Data Curation, Formal Analysis, Visualization, Writing – Original Draft; S.W.W. (First Author) and L.T. (First Author): Conceptualization, Methodology, Validation, Writing – Original Draft; W.L., P.J.Y., and W.X.Q.: Investigation and formal analysis; S.Y. and C.H.B.: Writing – Review and Editing; L.L. and Y.Y.: Resources; C.X.L. and L.Y.B.: Investigation; W.Y.B. (Corresponding Author): Conceptualization, Writing – review and editing, Supervision; Z.C. (Corresponding Author): Funding acquisition, Supervision; H.W.H. (Corresponding Author): Funding acquisition, Project administration, Supervision.

DECLARATION OF INTERESTS

There are no conflicts of interest to declare.

INCLUSION AND DIVERSITY

We support the inclusive, diverse, and equitable conduct of research.

Received: February 3, 2023
Revised: May 30, 2023
Accepted: July 6, 2023
Published: July 11, 2023

REFERENCES

1. Hunter, D.J. (2009). Risk stratification for knee osteoarthritis progression: a narrative review. Osteoarthritis Cartilage *17*, 1402–1407. https://doi.org/10.1016/j.joca.2009.04.014.

2. Jackson, D.W., Scheer, M.J., and Simon, T.M. (2001). Cartilage substitutes: overview of basic science and treatment options. J. Am. Acad. Orthop. Surg. *9*, 37–52. https://doi.org/10.5435/00124635-200101000-00005.

3. Redondo, M.L., Beer, A.J., and Yanke, A.B. (2018). Cartilage Restoration: Microfracture and Osteochondral Autograft Transplantation. J. Knee Surg. *31*, 231–238. https://doi.org/10.1055/s-0037-1618592.

4. Bradley, C.A. (2019). Opening up a pathway for disease modification in osteoarthritis. Nat. Rev. Drug Discov. *18*, 497. https://doi.org/10.1038/d41573-019-00098-5.

5. Armiento, A.R., Stoddart, M.J., Alini, M., and Eglin, D. (2018). Biomaterials for articular cartilage tissue engineering: Learning from biology. Acta Biomater. *65*, 1–20. https://doi.org/10.1016/j.actbio.2017.11.021.

6. Makris, E.A., Gomoll, A.H., Malizos, K.N., Hu, J.C., and Athanasiou, K.A. (2015). Repair and tissue engineering techniques for articular cartilage. Nat. Rev. Rheumatol. *11*, 21–34. https://doi.org/10.1038/nrrheum.2014.157.

7. Krishnan, Y., and Grodzinsky, A.J. (2018). Cartilage diseases. Matrix Biol. *71–72*, 51–69. https://doi.org/10.1016/j.matbio.2018.05.005.

8. Liu, Y., Liu, L., Wang, Z., Zheng, G., Chen, Q., and Luo, E. (2018). Application of Electrospinning Strategy on Cartilage Tissue Engineering. Curr. Stem Cell Res. Ther. *13*, 526–532. https://doi.org/10.2174/1574888X13666180628163515.

9. Han, Y., Yang, J., Zhao, W., Wang, H., Sun, Y., Chen, Y., Luo, J., Deng, L., Xu, X., Cui, W., and Zhang, H. (2021). Biomimetic injectable hydrogel microspheres with enhanced lubrication and controllable drug release for the treatment of osteoarthritis. Bioact. Mater. *6*, 3596–3607. https://doi.org/10.1016/j.bioactmat.2021.03.022.

10. Daly, A.C., Freeman, F.E., Gonzalez-Fernandez, T., Critchley, S.E., Nulty, J., and Kelly, D.J. (2017). 3D Bioprinting for Cartilage and Osteochondral Tissue Engineering. Adv. Healthc. Mater. *6*, 1700298. https://doi.org/10.1002/adhm.201700298.

11. Gu, Y., Zhang, L., Du, X., Fan, Z., Wang, L., Sun, W., Cheng, Y., Zhu, Y., and Chen, C. (2018). Reversible physical crosslinking strategy with optimal temperature for 3D bioprinting of human chondrocyte-laden gelatin methacryloyl bioink. J. Biomater. Appl. *33*, 609–618. https://doi.org/10.1177/0885328218805864.

12. Lin, L., Wang, Y., Wang, L., Pan, J., Xu, Y., Li, S., Huang, D., Chen, J., Liang, Z., Yin, P., et al. (2020). Injectable microfluidic hydrogel microspheres based on chitosan and poly (ethylene glycol) diacrylate (PEGDA) as chondrocyte carriers. RSC Adv. *10*, 39662–39672. https://doi.org/10.1039/d0ra07318k.

13. Mendes, B.B., Daly, A.C., Reis, R.L., Domingues, R.M.A., Gomes, M.E., and Burdick, J.A. (2021). Injectable hyaluronic acid and platelet lysate-derived granular hydrogels for biomedical applications. Acta Biomater. *119*, 101–113. https://doi.org/10.1016/j.actbio.2020.10.040.

14. Chen, J., Huang, D., Wang, L., Hou, J., Zhang, H., Li, Y., Zhong, S., Wang, Y., Wu, Y., and Huang, W. (2020). 3D bioprinted multiscale composite scaffolds based on gelatin methacryloyl (GelMA)/chitosan microspheres as a modular bioink for enhancing 3D neurite outgrowth and elongation. J. Colloid Interface Sci. *574*, 162–173. https://doi.org/10.1016/j.jcis.2020.04.040.

15. Wu, Y., Wang, L., Guo, B., and X Ma, P. (2014). Injectable biodegradable hydrogels and microgels based on methacrylated poly (ethylene glycol)-co-poly (glycerol sebacate) multi-block copolymers: synthesis, characterization, and cell encapsulation.

J. Mater. Chem. B *2*, 3674–3685. https://doi.org/10.1039/c3tb21716g.

16. Wang, L., Li, T., Wang, Z., Hou, J., Liu, S., Yang, Q., Yu, L., Guo, W., Wang, Y., Guo, B., et al. (2022). Injectable remote magnetic nanofiber/hydrogel multiscale scaffold for functional anisotropic skeletal muscle regeneration. Biomaterials *285*, 121537. https://doi.org/10.1016/j.biomaterials.2022.121537.

17. Zhang, X., Yan, Z., Guan, G., Lu, Z., Yan, S., Du, A., Wang, L., and Li, Q. (2022). Polyethylene glycol diacrylate scaffold filled with cell-laden methacrylamide gelatin/alginate hydrogels used for cartilage repair. J. Biomater. Appl. *36*, 1019–1032. https://doi.org/10.1177/08853282211044853.

18. Kaklamani, G., Cheneler, D., Grover, L.M., Adams, M.J., and Bowen, J. (2014). Mechanical properties of alginate hydrogels manufactured using external gelation. J. Mech. Behav. Biomed. Mater. *36*, 135–142. https://doi.org/10.1016/j.jmbbm.2014.04.013.

19. Ma, C., Choi, J.B., Jang, Y.S., Kim, S.Y., Bae, T.S., Kim, Y.K., Park, J.M., and Lee, M.H. (2021). Mammalian and Fish Gelatin Methacryloyl-Alginate Interpenetrating Polymer Network Hydrogels for Tissue Engineering. ACS Omega *6*, 17433–17441. https://doi.org/10.1021/acsomega.1c01806.

20. Xiao, S., Zhao, T., Wang, J., Wang, C., Du, J., Ying, L., Lin, J., Zhang, C., Hu, W., Wang, L., and Xu, K. (2019). Gelatin Methacrylate (GelMA)-Based Hydrogels for Cell Transplantation: an Effective Strategy for Tissue Engineering. Stem Cell Rev. Rep. *15*, 664–679. https://doi.org/10.1007/s12015-019-09893-4.

21. Yue, K., Trujillo-de Santiago, G., Alvarez, M.M., Tamayol, A., Annabi, N., and Khademhosseini, A. (2015). Synthesis, properties, and biomedical applications of gelatin methacryloyl (GelMA) hydrogels. Biomaterials *73*, 254–271. https://doi.org/10.1016/j.biomaterials.2015.08.045.

22. Engbert, A., Gruber, S., and Plank, J. (2020). The effect of alginates on the hydration of calcium aluminate cement. Carbohydr. Polym. *236*, 116038. https://doi.org/10.1016/j.carbpol.2020.116038.

23. Wang, T., Lai, J.H., and Yang, F. (2016). Effects of Hydrogel Stiffness and Extracellular Compositions on Modulating Cartilage Regeneration by Mixed Populations of Stem Cells and Chondrocytes In Vivo. Tissue Eng. *22*, 1348–1356. https://doi.org/10.1089/ten.TEA.2016.0306.

24. Martyniak, K., Lokshina, A., Cruz, M.A., Karimzadeh, M., Kemp, R., and Kean, T.J. (2022). Biomaterial composition and stiffness as decisive properties of 3D bioprinted constructs for type II collagen stimulation. Acta Biomater. *152*, 221–234. https://doi.org/10.1016/j.actbio.2022.08.058.

25. Bachmann, B., Spitz, S., Schädl, B., Teuschl, A.H., Redl, H., Nürnberger, S., and Ertl, P. (2020). Stiffness Matters: Fine-Tuned Hydrogel Elasticity Alters Chondrogenic Redifferentiation. Front. Bioeng. Biotechnol. *8*, 373. https://doi.org/10.3389/fbioe.2020.00373.

26. Cheng, X., Yin, P., Li, T., Luo, L., Yang, Y., Wang, L., Su, W., Wang, Y., Li, Y., Wang, Y., et al. (2022). Injectable composite hydrogels encapsulating gelatin methacryloyl/chitosan microspheres as ARPE-19 cell transplantation carriers. Biomater. Sci. *11*, 278–287. https://doi.org/10.1039/d2bm01413k.

27. Helgeson, M.E., Chapin, S.C., and Doyle, P.S. (2011). Hydrogel microparticles from lithographic processes: novel materials for fundamental and applied colloid science. Curr. Opin. Colloid Interface Sci. *16*, 106–117. https://doi.org/10.1016/j.cocis.2011.01.005.

28. Naqvi, S.M., Vedicherla, S., Gansau, J., McIntyre, T., Doherty, M., and Buckley, C.T. (2016). Living Cell Factories - Electrosprayed Microcapsules and Microcarriers for Minimally Invasive Delivery. Adv. Mater. *28*, 5662–5671. https://doi.org/10.1002/adma.201503598.

29. Sinclair, A., O'Kelly, M.B., Bai, T., Hung, H.C., Jain, P., and Jiang, S. (2018). Self-Healing Zwitterionic Microgels as a Versatile Platform for Malleable Cell Constructs and Injectable Therapies. Adv. Mater. *30*, e1803087. https://doi.org/10.1002/adma.201803087.

30. Daly, A.C., Riley, L., Segura, T., and Burdick, J.A. (2020). Hydrogel microparticles for biomedical applications. Nat. Rev. Mater. *5*, 20–43. https://doi.org/10.1038/s41578-019-0148-6.

31. Zhao, X., Liu, S., Yildirimer, L., Zhao, H., Ding, R., Wang, H., Cui, W., and Weitz, D. (2016). Injectable stem cell-laden photocrosslinkable microspheres fabricated using microfluidics for rapid generation of osteogenic tissue constructs. Adv. Funct. Mater. *26*, 2809–2819. https://doi.org/10.1002/adfm.201504943.

32. Wong, C.Y., Al-Salami, H., and Dass, C.R. (2018). Microparticles, microcapsules and microspheres: A review of recent developments and prospects for oral delivery of insulin. Int. J. Pharm. *537*, 223–244. https://doi.org/10.1016/j.ijpharm.2017.12.036.

33. Xie, M., Gao, Q., Zhao, H., Nie, J., Fu, Z., Wang, H., Chen, L., Shao, L., Fu, J., Chen, Z., and He, Y. (2019). Electro-Assisted Bioprinting of Low-Concentration GelMA Microdroplets. Small *15*, e1804216. https://doi.org/10.1002/smll.201804216.

34. Wang, G., An, Y., Zhang, X., Ding, P., Bi, H., and Zhao, Z. (2021). Chondrocyte Spheroids Laden in GelMA/HAMA Hybrid Hydrogel for Tissue-Engineered Cartilage with Enhanced Proliferation, Better Phenotype Maintenance, and Natural Morphological Structure. Gels *7*, 247. https://doi.org/10.3390/gels7040247.

35. George, E., Jahan, I., Barai, A., Ganesan, V., and Sen, S. (2021). High ligand density drives extensive spreading and motility on soft GelMA gels. Biomed. Mater. *16*, 054103. https://doi.org/10.1088/1748-605X/ac177b.

36. Sridhar, B.V., Doyle, N.R., Randolph, M.A., and Anseth, K.S. (2014). Covalently tethered TGF-β1 with encapsulated chondrocytes in a PEG hydrogel system enhances extracellular matrix production. J. Biomed. Mater. Res. *102*, 4464–4472. https://doi.org/10.1002/jbm.a.35115.

37. Biondo, M., Panuzzo, C., Ali, S.M., Bozzaro, S., Osella, M., Bracco, E., and Pergolizzi, B. (2021). The Dynamics of Aerotaxis in a Simple Eukaryotic Model. Front. Cell Dev. Biol. *9*, 720623. https://doi.org/10.3389/fcell.2021.720623.

38. Colton, C.K. (2014). Oxygen supply to encapsulated therapeutic cells. Adv. Drug Deliv. Rev. *67–68*, 93–110. https://doi.org/10.1016/j.addr.2014.02.007.

39. Van de Walle, A., Wilhelm, C., and Luciani, N. (2017). 3D Magnetic Stem Cell Aggregation and Bioreactor Maturation for Cartilage Regeneration. J. Vis. Exp. *55221*, 55221. https://doi.org/10.3791/55221.

40. Motoike, S., Kajiya, M., Komatsu, N., Takewaki, M., Horikoshi, S., Matsuda, S., Ouhara, K., Iwata, T., Takeda, K., Fujita, T., and Kurihara, H. (2018). Cryopreserved clumps of mesenchymal stem cell/extracellular matrix complexes retain osteogenic capacity and induce bone regeneration. Stem Cell Res. Ther. *9*, 73. https://doi.org/10.1186/s13287-018-0826-0.

41. Li, T., Hou, J., Wang, L., Zeng, G., Wang, Z., Yu, L., Yang, Q., Yin, J., Long, M., Chen, L., et al. (2023). Bioprinted anisotropic scaffolds with fast stress relaxation bioink for engineering 3D skeletal muscle and repairing volumetric muscle loss. Acta Biomater. *156*, 21–36. https://doi.org/10.1016/j.actbio.2022.08.037.

42. Li, Q., Zhang, B., Xue, Q., Zhao, C., Luo, Y., Zhou, H., Ma, L., Yang, H., and Bai, D. (2021). A Systematic Thermal Analysis for Accurately Predicting the Extrusion Printability of Alginate-Gelatin-Based Hydrogel Bioinks. Int. J. Bioprint. *7*, 394. https://doi.org/10.18063/ijb.v7i3.394.

43. Hong, H., Seo, Y.B., Kim, D.Y., Lee, J.S., Lee, Y.J., Lee, H., Ajiteru, O., Sultan, M.T., Lee, O.J., Kim, S.H., and Park, C.H. (2020). Digital light processing 3D printed silk fibroin hydrogel for cartilage tissue engineering. Biomaterials *232*, 119679. https://doi.org/10.1016/j.biomaterials.2019.119679.

44. Wu, X., Guo, W., Wang, L., Xu, Y., Wang, Z., Yang, Y., Yu, L., Huang, J., Li, Y., Zhang, H., et al. (2021). An Injectable Asymmetric-Adhesive Hydrogel as a GATA6+ Cavity Macrophage Trap to Prevent the Formation of Postoperative Adhesions after Minimally Invasive Surgery. Adv. Funct. Mater. *32*, 2110066. https://doi.org/10.1002/adfm.202110066.

45. Anderson, J.M., Rodriguez, A., and Chang, D.T. (2008). Foreign body reaction to biomaterials. Semin. Immunol. *20*, 86–100. https://doi.org/10.1016/j.smim.2007.11.004.

46. Ibrahim, M., Bond, J., Medina, M.A., Chen, L., Quiles, C., Kokosis, G., Bashirov, L., Klitzman, B., and Levinson, H. (2017). Characterization

of the Foreign Body Response to Common Surgical Biomaterials in a Murine Model. Eur. J. Plast. Surg. *40*, 383–392. https://doi.org/10.1007/s00238-017-1308-9.

47. Yi, H.G., Choi, Y.J., Jung, J.W., Jang, J., Song, T.H., Chae, S., Ahn, M., Choi, T.H., Rhie, J.W., and Cho, D.W. (2019). Three-dimensional printing of a patient-specific engineered nasal cartilage for augmentative rhinoplasty. J. Tissue Eng. *10*, 2041731418824797. https://doi.org/10.1177/2041731418824797.

48. Wang, L., Wu, Y., Hu, T., Ma, P.X., and Guo, B. (2019). Aligned conductive core-shell biomimetic scaffolds based on nanofiber yarns/hydrogel for enhanced 3D neurite outgrowth alignment and elongation. Acta Biomater. *96*, 175–187. https://doi.org/10.1016/j.actbio.2019.06.035.

49. Wang, S., Guan, S., Zhu, Z., Li, W., Liu, T., and Ma, X. (2017). Hyaluronic acid doped-poly(3,4-ethylenedioxythiophene)/chitosan/gelatin (PEDOT-HA/Cs/Gel) porous conductive scaffold for nerve regeneration. Mater. Sci. Eng. C Mater. Biol. Appl. *71*, 308–316. https://doi.org/10.1016/j.msec.2016.10.029.

50. Zhang, J., Xu, W., Xu, F., Lu, W., Hu, L., Zhou, J., Zhang, C., and Jiang, Z. (2021). Microfluidic droplet formation in co-flow devices fabricated by micro 3D printing. J. Food Eng. *290*, 110212. https://doi.org/10.1016/j.jfoodeng.2020.110212.

51. Cai, N., Li, Q., Zhang, J., Xu, T., Zhao, W., Yang, J., and Zhang, L. (2017). Antifouling zwitterionic hydrogel coating improves hemocompatibility of activated carbon hemoadsorbent. J. Colloid Interface Sci. *503*, 168–177. https://doi.org/10.1016/j.jcis.2017.04.024.

52. Chae, S., Lee, S.S., Choi, Y.J., Hong, D.H., Gao, G., Wang, J.H., and Cho, D.W. (2021). 3D cell-printing of biocompatible and functional meniscus constructs using meniscus-derived bioink. Biomaterials *267*, 120466. https://doi.org/10.1016/j.biomaterials.2020.120466.

STAR★METHODS

KEY RESOURCES TABLE

REAGENT or RESOURCE	SOURCE	IDENTIFIER
Antibodies		
Goat anti-Rabbit IgG (H+L)	Antibody Registry	RRID: AB_2337910
Goat anti-Mouse IgG (H+L)	Antibody Registry	RRID: AB_2338443
Rabbit Anti-SOX9 Polyclonal Antibody	Antibody Registry	RRID: AB_11456645
Rabbit Anti-Collagen I Polyclonal Antibody	Antibody Registry	RRID: AB_374559
Rabbit Anti-Collagen II Polyclonal Antibody	Antibody Registry	RRID: AB_374560
Rabbit Anti-ACAN Polyclonal Antibody	Antibody Registry	RRID: AB_11353338
Chemicals, peptides, and recombinant proteins		
Gelatin from porcine skin	Sigma-Aldrich	V900863 Cat# 9000-70-8
Methacrylic anhydride	Sigma-Aldrich	276685 Cat# 760-93-0
Sodium alginate	aladdin	S100128 Cat# 9005-38-3
Calcium chloride	Sigma-Aldrich	V900266 Cat# 10043-52-4
Mineral oil	aladdin	M195121 Cat# 8020-83-5
Dimethyl sulfoxide	aladdin	D103272 Cat# 67-68-5
Glycerol	Sigma-Aldrich	V900122 Cat# 56-81-5
Paraformaldehyde	Sigma-Aldrich	158127 Cat# 30525-89-4
Span 80	aladdin	S110839-1l Cat# 1338-43-8
Blue Light Initiator (LAP)	StemEasy	SE-3DP-0100
Trizol	Life Technologies	15596026
Fetal Bovine Serum	Gibco	10270106
Dulbecco's modified eagle medium	Gibco	C11995500BT
Triton X-100	Sigma-Aldrich	V900502
Critical commercial assays		
alamarBlue™ Cell Viability Reagent	Thermo Fisher	DAL1025
Bovine Serum Albumin	Meilunbio	V900933
LIVE/DEAD VIABILITY/CY 1 KIT	Invitrogen	L3224
HE staining kit	Solarbio	G1120
CELLTRACKER RED CMTPX	Thermo Fisher	C34552
Pierce™ BCA Protein Assay Kit	Thermo Fisher	23227
DAPI	Sigma-Aldrich	D9542
Experimental models: Cell lines		
Primary chondrocytes of the knee	This paper	N/A
Experimentalmodels:Organisms/strain		
Sprague Dawley rats	the Guangdong Provincial Animal Center	N/A

(*Continued on next page*)

Continued

REAGENT or RESOURCE	SOURCE	IDENTIFIER
BALB/c Nude mice	the Guangdong Provincial Animal Center	N/A
Software and algorithms		
Image J	NIH	https://imagej.nih.gov/ij/download.html
Origin	OriginLab	https://www.originlab.com
IBM SPSS Statistics	IBM	https://www.ibm.com/products/spss-statistics
ZEN	ZEISS	https://www.zeiss.com
Other		
Fourier Transform infrared spectroscopy, FT-IR	PerkinElmer	Frontier FT-IR/NIR/FIR; https://chem.washington.edu/instruments/perkin-elmer-frontier-ftir
Nuclear Magnetic Resonance, NMR	BRUKER	AVANCE-III HD 400 MHz; https://pharm.ucsf.edu/nmr/instruments/bruker-400

RESOURCE AVAILABILITY

Lead contact

Further information and requests for resources and reagents should be directed to and will be fulfilled by the Lead Contact, Yaobin Wu (wuyaobin2018@smu.edu.cn).

Materials availability

This study did not generate new unique reagents.

Data and code availability

- Data reported in this paper will be shared by the lead contact upon request.
- This paper does not report original code.
- Any additional information required to reanalyze the data reported in this paper is available from the lead contact upon request.

EXPERIMENTAL MODEL AND STUDY PARTICIPANT DETAILS

Animals

The healthy experimental animals including 6-week-old female SD rats and 4-week-old female nude mice were purchased from the Guangdong Provincial Animal Center, which did not involve in any procedures or drug test. The animal experiments were approved by the Guangdong Provincial Animal Ethics Committee. These animals in this study were housed in an animal house under appropriate humidity and temperature (relative humidity: 50%-60%; room temperature: 23°C-25°C), with unrestricted access to water and food. Furthermore, the rats and mice after implantation of the scaffolds were transferred to the previous animal house for feeding.

Cell culture

Chondrocytes were obtained from the knee cartilage of 5-day-old SD rats. Chondrocytes were cultured in a Petri dish (100 mm) with Dulbecco's modified Eagle's medium (DMEM) containing penicillin (100 U/mL), streptomycin (100 U/mL), and 10% fetal bovine serum (FBS). The cells were cultured under 5% CO_2 at 37°C.

METHOD DETAILS

Preparation and characterization of GelMA and GelMA/alginate (GA) hydrogels

The synthetic method for GelMA was optimized following our previous study.[48] Briefly, methacrylic anhydride (MA, 20% v/v) was added in a flask containing gelatin solution (10% w/v) by heating and stirring for 3 h. Then, the reaction solution was added to anhydrous ethanol for precipitation to remove MA byproducts, and the precipitate was dissolved in deionized water at 50°C. The resulting solution was dialyzed in deionized water at 50°C for 3 days to obtain product. The structures of the gelatin and GelMA hydrogels were

characterized by ^{1}H-NMR spectroscopy (600 MHz, AVANCE IIITM HD, Bruker). Fourier transform infrared (FT-IR) spectra (NICOLET 6700, Thermos) of the GelMA, alginate, and lyophilized GA solutions were recorded from 1000 to 4000 cm^{-1}. The degree of substitution of GelMA was calculated using the ninhydrin reaction because the amino groups of GelMA react with ninhydrin to form a purple compound upon heating.

For the preparation of the bioinks, different concentrations of GelMA (5%, 10%, or 15% (w/v)) were added to the sample bottles containing alginate solution (1.2% w/v) and lithium phenyl-2,4,6-trimethylbenzoyl-phosphinate solution (LAP, 0.2% w/v) to prepare different GA precursor solutions. The solution was gelation under UV light (365 nm, 7 mW/cm^2) for 15 s and then immersed in a calcium chloride solution (200 mmol/L) for 30 s for secondary cross-linking, thus yielding the GA hydrogel. The swelling (*S*) and degradation (*D*) properties of the hydrogels were assessed by immersing the hydrogels in PBS.[49] This was done by obtaining the initial weight (W_o) of the lyophilized cylindrical hydrogels and then immersing them in PBS and re-weighing them every 5 min (W_i). Before weighing, any water on the surface of the hydrogel was gently removed with blotting paper. The formula for calculating the swelling rate is as follows:

$$S(\%) = (W_o - W_t) / W_i \times 100\%.$$

In addition, after lyophilization, the cylindrical hydrogels were immersed in PBS and weighed weekly (W_t). The formula for calculating the degradation rate is as follows:

$$D(\%) = (W_o - W_t) / W_o \times 100\%.$$

The shear viscosity of the GA hydrogels was measured using a rheometer (HAAKE MARS 40, Thermo Fisher).

In addition, GelMA (5% w/v), alginate (1.2% w/v), and GelMA (5% w/v)/alginate (1.2% w/v) (denoted GA) were dissolved in deionized water with heating and stirring at 40°C to obtain the respective precursor solutions, which were gelated using UV light and calcium chloride solution. Rheological evaluation of the GelMA, alginate, and GA hydrogels was performed using a rheometer (HAAKE MARS 40, Thermo Fisher), while the storage modulus (*G'*) and the loss modulus (*G"*) of the hydrogels were obtained by oscillatory scanning tests with angular frequencies in the range of 0.1–10 Hz and a rotation amplitude of 1%. The pore size and porosity of the freeze-dried GelMA hydrogels (5%, 10%, and 15% w/v) were observed via scanning electron microscopy (SEM) (Hitachi S-3000, thickness: 10 nm).

Multichannel microfluidic chip design and fabrication

A multichannel microfluidic chip was fabricated using a microscale 3D printing device. The parameters of the multichannel microfluidic chip were set using the Pore program. After the STL model file had been imported into the computer, printing was carried out using photosensitive resin as the primary material.

Because of flow resistance, the water phase should be subjected to different pressures at the entrances of the channels in the chip. However, Jiang et al. have reported that the effect of the pressure difference at the entrance of the interphase channels can be neglected.[50]

Fabrication of GelMA (G-MS), alginate (A-MS), and GelMA/alginate (GA-MS) microspheres

The GelMA, alginate, and GelMA/alginate aqueous precursor solutions were drawn into a 1-mL syringe, respectively, whereas the oil-phase solution was prepared by mixing liquid paraffin with Span 80 in a 19:1 volume ratio and drawn into a 20-mL syringe. The microspheres were fabricated by installing both syringes on an injection pump, connecting the microfluidic chip to the syringes with silicone hoses, and starting the injection pump. The microspheres were collected at the outlet of the microfluidic chip. G-MS was collected in a centrifugal tube containing Dulbecco's buffered saline (DPBS) after UV irradiation for 15 s, whereas A-MS and GA-MS were collected in centrifugal tubes containing calcium chloride solution for gelation, although the latter was collected after UV irradiation for 15 s. The microspheres collected in the centrifugal tubes were centrifuged (2000 rpm/min for 5 min), washed with DPBS, and observed using an optical microscope (BX53F, Olympus). Subsequently, particle size analysis was carried out using ImageJ (NIH). To explore the influence of different flow rates of the water and oil phases on the microsphere diameter, the flow rates of the water and oil phase solutions were set to 5, 10, and 15 μL/min and 300, 600, 900, 1200, and 1500 μL/min, respectively. Fluorescein isothiocyanate (FITC) was added to the water phase to

allow the microspheres to be observed via fluorescence microscopy (BX53F, Olympus). The microsphere diameter was measured using ImageJ (NIH) and analyzed in OriginPro. To observe the surface microscopic properties of GA-MS, the microspheres were dehydrated using gradient alcohol, surface-coated with gold, and then observed via SEM (Hitachi S-3000, thickness: 10 nm).

Sustained release of BSA-FITC and BSA within GA-MS

The sustained-release properties of GA-MS were analyzed qualitatively and quantitatively by fabricating GA-MS encapsulating BSA-FITC and BSA alone, respectively. In detail, BSA-FITC (400 μg/mL) was added to the GelMA/alginate precursor solution to fabricate the GA-MS. The GA-MS encapsulating BSA-FITC was centrifuged at 2000 rpm for 3 min, washed with deionized water three times, and immersed in DPBS. The images of the GA-MS were taken 0, 3, 9, 21, and 36 h after immersion using a confocal laser microscope (LSM800, Zeiss) and converted to grayscale images using ImageJ. Using the grayscale 3D heat maps, the size distribution histograms were plotted and used to calculate the means and standard deviations of the gray levels at each statistical time point using ImageJ and OriginPro. The addition of BSA (40 mg/mL) alone to the GA precursor solution was used to explore the difference in the sustained-release properties of GA-MS having different diameters. Specifically, GA-MS with diameters of 457 $\pm$ 3, 361 $\pm$ 4, and 246 $\pm$ 6 μm were prepared and immersed in 200 μL of DPBS in the wells of a 96-well plate, and the numbers of microspheres per well were 5, 11, and 33, respectively, meaning that the total mass of BSA in each group was similar. The sustained release of BSA in GA-MS at 0, 0.5, 1, 2, and 3 h was determined using a microplate reader with a bicinchoninic acid assay (BCA) working solution. DPBS was added after each measurement to compensate for volume loss.

Spreading ability of chondrocytes in the GelMA hydrogel

Chondrocytes were obtained from the knee cartilage of 5-day-old SD rats. Briefly, Rats were sacrificed and sterilized by immersion in alcohol. The articular cartilage was exposed in the ultra-clean table, which was cut out and transferred to the culture dish. Then the cartilage in the culture dish was digested with type II collagenase solution (0.1% w/v), and transferred to an incubator (37°C, 5% CO_2) for digestion overnight. Chondrocytes were obtained by centrifuging the digest at 1000 rpm/min for 5 min.

To explore the effect of different concentrations of the GelMA hydrogel on the spreading ability of the chondrocytes, the digested chondrocytes were cultured in GelMA hydrogel prepared from GelMA precursor solutions (5%, 10%, and 15% (w/v)). The precursor was heated to 70°C and filtered through a bacterial filter to obtain a sterile solution, then mixed with chondrocytes at a density of 1×10^5 cells/mL, and then blown evenly with a pipette gun. The 30-μL solution containing chondrocytes was added dropwise onto a petri dish and gelated under UV light for 15 s. The culture medium was then added to the Petri dish, which was transferred to an incubator for culture (37°C, 5% CO_2). After 3 days, the chondrocytes in the GelMA hydrogel were fixed with paraformaldehyde (4% w/v) for 30 min, permeabilized with Triton X-100 (0.25% v/v) for 10 min, and stained with phalloidin-FITC and 4′,6-diamidino-2-phenylindole (DAPI).

In-vitro biological characterization of cell-encapsulated GA-MS

The GelMA (5% w/v)/alginate (1.2% w/v) precursor solution was sterilized before the addition of chondrocytes. This was done by filtering the GelMA precursor solution (10% w/v) containing LAP (0.4% w/v) and TGF-β (20 μg/mL) through a bacterial filter, and by sterilizing the alginate precursor solution (2.4% w/v) by autoclaving. The two precursor solutions were then mixed in a 1:1 volume ratio and used as the water phase.

The chondrocyte-encapsulating GA-MS were washed three times with DPBS and cultured in a petri dish after centrifugation. The viability of the chondrocytes in GA-MS was measured using the Live/Dead Cell Staining Kit (Invitrogen), which uses calcein-AM and ethidium homodimer. Finally, images of the chondrocyte-encapsulating GA-MS were taken after 1 and 4 days of culture using a confocal laser microscope (LSM800, Zeiss) and converted to grayscale images using ImageJ to calculate the chondrocyte survival rate. Chondrocyte proliferation in GA-MS was determined using the Amar blue assay after 1, 4, and 7 days of culture.

The proteins secreted by the chondrocytes in GA-MS were stained after culturing for 5 days, as per the manufacturer's instructions. Briefly, the chondrocyte-encapsulating GA-MS were washed with DPBS three times, fixed with paraformaldehyde (4% w/v) for 30 min, permeabilized with Triton X-100 (0.25% v/v) for

10 min, and blocked with BSA solution (1% w/v) for 60 min. The chondrocyte-encapsulating GA-MS were then immersed in BSA solution containing monoclonal antibodies for aggrecan (ACAN), type-II collagen (COL II), and SOX 9, and incubated overnight at 4°C. The next day, after washing with DPBS three times, the chondrocyte-encapsulating GA-MS were incubated in BSA solution containing goat anti-mouse secondary antibody Alexa Fluor 594 (Invitrogen, USA) for 1 h. Subsequently, the chondrocyte-encapsulating GA-MS were incubated in a DAPI solution for 5 min. The images of the stained chondrocyte-encapsulating GA-MS were obtained using a confocal laser microscope (LSM800, Zeiss).

The chondrocyte-encapsulating GA-MS were collected and centrifuged, washed with DPBS three times, transferred to a cryopreservation tube containing 1 mL of CELLSAVING™ (NCM), and stored at −80°C for later use. The chondrocyte-encapsulating GA-MS that had been cryopreserved for 7 days were reactivated at 37°C within 1 min and diluted with Dulbecco's Modified Eagle Medium (DMEM) culture medium (9 mL) to prevent the chondrocytes from being harmed by the cryonic solution; they were then cultured in an incubator (37°C, 5% CO_2) for 5 days. The cell viability, proliferation, and protein secretion of the chondrocytes in GA-MS after cryopreservation and resuscitation were measured by the methods described in .6.2.

Preparation and rheological property of the Carbopol support bath

NaOH powder (40 mg) was dissolved in deionized water (100 mL) as the initial solution. Subsequently, Carbopol powder (0.2, 0.7, or 1.2 wt %) was added to the initial solution and the solution was stirred for 15 min to yield the Carbopol support bath; this was then transferred to 60-mm culture dishes for later use. The viscosity of different concentrations of the Carbopol support bath was tested using a rheometer at shear rates of 0.1–10 s^{-1} at room temperature.

Composite hydrogel printing based on Carbopol support bath

A GelMA (15% w/v)/alginate (1.2% w/v) precursor solution containing LAP (0.2% w/v) was prepared and loaded into the printing cylinder as the bioink, degassed in a vacuum drying oven, and cooled to 21°C for later use. To explore the dimensional stability of the bioink, the bioink was extruded into a Carbopol support bath under different conditions (temperature, extrusion pressure, printing speed, and needle diameter) using the 3D bioprinter (EnvisionTec, 3D-Bioplotter Developer Series). Concerning these parameters, the tested temperatures were 14, 21, and 28°C, the tested extrusion pressures were 3.0, 3.5, and 4.0 bar, the tested printing speeds were 5.0, 8.0, and 11.0 mm/s, and the tested needle diameters were 21G, 22G, and 24G. To explore the accuracy of bioink printing in the Carbopol support bath, the bioink was extruded into the Carbopol support bath to prepare 3D models of circles and pentacles.

Construction of 3D multiscale composite scaffolds in the Carbopol support bath

The GA-MS were added to the GelMA/alginate precursor solution containing LAP (0.2% w/v) as a multifunctional GA-MS–GelMA/alginate modular bioink. To enable the observation of the morphology of the multiscale composite scaffolds better, GA-MS was dyed with FITC, and the GelMA/alginate precursor solution was dyed red with rhodamine. The modular bioink was then extruded into the Carbopol support bath by the 3D bioprinter to yield multiscale composite scaffolds that were first gelated under UV light for 15 s and then crosslinked in aqueous calcium chloride. Calcium chloride dissolved the Carbopol support bath leaving behind the multiscale composite scaffolds. The multiscale composite scaffolds were then dehydrated using gradient alcohol, surface-coated with gold, and observed under different magnifications via scanning electron microscopy (SEM, Hitachi S-3000, thickness: 10 nm). Fluorescence and white light images of the composite scaffolds were obtained using a stereomicroscope (Stemi2000-C, Zeiss), and a confocal laser microscope (LSM800, Zeiss) was used to obtain the images of the GA-MS distribution in the multiscale composite scaffolds. The images were converted to grayscale using ImageJ. To track the distribution of the chondrocytes encapsulated in GA-MS within the composite scaffolds, the chondrocyte membranes were labeled with Cell Tracker Red CMTPX Dye (DIO, Beyotime, Shanghai) before encapsulation in the GA-MS. The multiscale composite scaffolds containing chondrocyte-encapsulating GA-MS were observed via a confocal laser microscope (LSM800, Zeiss).

Hemolysis rate (HR) of materials

Fresh blood (5 mL) was collected from Sprague–Dawley (SD) rats and added to an anticoagulant tube containing PBS (5 mL) to dilute the blood in a 1:1 volume ratio. Then, a sample of GelMA, alginate, or

GA (200 mg) was added to test tubes containing sterile PBS (5 mL), and the test tubes were incubated at 37°C for 30 min. In addition, deionized water (5 mL) and PBS (5 mL) were used as positive and negative controls, respectively. Subsequently, the diluted blood (200 μL) was added to the test tubes containing GelMA, alginate, or GA, after which the tubes were incubated at 37°C for 1 h and then centrifuged at 3500 rpm for 5 min. The HR was calculated by measuring the absorbance of the supernatant at 545 nm in each test tube and using the following formula: $HR = (OD_1 - OD_0)/(OD_2 - OD_0) \times 100\%$, where OD_0, OD_1, and OD_2 are the absorbances of the negative control, samples, and positive control, respectively.[44,51]

In-vivo investigation of the 3D multiscale composite scaffolds

GelMA (15% w/v), alginate (1.2% w/v), and GelMA (15% w/v)/alginate (1.2% w/v) precursor solutions were loaded into a printing cylinder for use as bioinks and used to prepare 3D-printed scaffolds (5 mm × 5 mm × 1 mm). After preparation, the scaffolds were implanted into the subcutaneous tissue of SD rats. Four SD rats each were implanted with the scaffolds from the three groups, including the GelMA group, alginate group, and GM-alg group. The biocompatibility of the materials was investigated by evaluating the hematoxylin and eosin (HE) staining and F4/80 immunohistochemical fluorescence staining of the scaffolds. In more detail, 6-week-old female SD rats were used, and samples were taken after 1-, 2-, 3-, and 4-weeks post-implantation of the composite scaffolds. For implantation, the rats were anesthetized by the intraperitoneal injection of pentobarbital sodium (1%, 0.6 mL/100g), and then the 3D-printed scaffolds were implanted into the subcutaneous bag. Subsequently, the 3D-printed scaffolds were retrieved from the surrounding tissue after 1-, 2-, 3-, and 4-weeks post implantation. The samples were fixed with 4% formaldehyde, dehydrated, embedded in paraffin, and then cut into 8-μm-thick slices using a slicer. The sections were stained with HE dyes to observe the biocompatibility and degradability of the material *in vivo*, and visualization was carried out using an optical microscope (BX53F, Olympus).

In addition, scaffold sections were stained with F4/80 immunofluorescent dye to count the macrophages around the scaffolds.[52] A working solution was prepared by mixing F4/80 antibody stock solution (1 μL) with 10% donkey serum (50 μL), and this solution was then added dropwise onto the scaffold sections, which were then incubated at 4°C overnight. On the next day, these sections were washed with TBST (Tris-HCl, NaCl, and Tween 20) three times, and donkey anti-rabbit (594) secondary antibody working solution, which was prepared by mixing Alexa Fluor®594 Donkey anti-Rabbit IgG (H+L) stock solution (1 μL) with TBST (400 μL), was added, and the section was incubated at 37°C for 45 min. The sections were then stained with DAPI for 5 min and observed using confocal fluorescence microscopy (BX53F, Olympus). Four different images were obtained for each section, and the mean number of macrophages was calculated.

Chondrocytes were obtained from the knee cartilage of 5-day-old SD rats and added to the GelMA (5% w/v)/alginate (1.2% w/v) precursor solution to prepare chondrocyte-encapsulating GA-MS, which were cryopreserved for later use. When the number of the cryopreserved GA-MS containing chondrocytes was sufficient for printing, they were reactivated and mixed with sterile GelMA (15% w/v)/alginate (1.2% w/v) precursor solution to fabricate the multiscale composite scaffolds. The scaffolds were then implanted into 4-week-old female nude mice using the protocols described in Section 2.11.1. Eight mice each were implanted with the scaffolds containing microsphere-embedded chondrocytes. Subsequently, samples were taken 2 and 4 weeks after 3D multiscale composite scaffold implantation. These samples were then fixed with 4% formaldehyde, dehydrated, embedded in wax blocks, and cut into 8-μm-thick sections using a slicer. Additionally, these sections were immunohistologically stained for aggrecan (ACAN), type-I collagen (COL I), type-II collagen (COL II), and SOX 9. Images of chondroblast expression of chondrocytes in GA-MS within the multiscale composite scaffolds were obtained using optical microscopy (BX53F, Olympus).

QUANTIFICATION AND STATISTICAL ANALYSIS

Experiments were run at least three times for each sample ($n \geq 3$ per sample), and the experimental data are reported as the mean ± standard deviation (SD), as calculated using IBM SPSS Statistics. All the statistical details of experiments can be found in figure legends and Results. One-way analysis of variance (-ANOVA) was used to analyze the significance of the observed differences between the study groups and $p < 0.05$ was considered statistically significant.